Article

Energy-Efficient beyond 5G Multiple Access Technique with Simultaneous Wireless Information and Power Transfer for the Factory of the Future

Zaid Albataineh [1], **Admoon Andrawes [2]**, **Nor Fadzilah Abdullah [2,*]** and **Rosdiadee Nordin [2]**

1   Department of Electronics Engineering, Yarmouk University, Irbid 21163, Jordan
2   Department of Electrical, Electronic & Systems Engineering, Faculty of Engineering and Built Environment, Universiti Kebangsaan Malaysia, Bangi 43600, Malaysia
*   Correspondence: fadzilah.abdullah@ukm.edu.my

Abstract: In the Industrial Internet of Things (IIoT), non-orthogonal multiple access (NOMA) has emerged as a viable multiple access method due to its superior efficiency. In this paper, a new power allocation technique for NOMA-enabled IIoT devices is presented with trade-offs between increasing energy efficiency and decreasing power consumption. We present a joint optimization of transmission rate and energy harvesting in simultaneous wireless information and power transfer (SWIPT) NOMA-enabled IIoT devices. With the power splitting (PS) approach, we examine how to improve overall transmission rate and harvested energy, simultaneously, while fulfilling the minimum rate and harvested energy needs of each IIoT device in a SWIPT-enabled NOMA system. An objective function is established by adding transmission rates obtained from information decoding and the transformed throughput from energy harvesting. The combination of management approaches with Industry 4.0 technology provides a viable strategy to decrease industrial production's energy use. Several performance metrics may be utilized to study manufacturing process optimization. The efficiency of production equipment may be measured by looking at the overall effectiveness (OE) of the equipment in use. We divide the non-convex optimization problem into two sub-problems, based on the Lagrangian duality method, and solve them to find the optimal solution for the non-convex problem. The approach is validated based on physical layer parameter settings that represent potential factory of the future scenarios. Simulation results confirm the effectiveness of the presented method in a SWIPT-enabled NOMA system, provide considerable performance gains over the classic rate maximization strategy, and demonstrate the energy efficiency of the presented method compared with the conventional system. The results show huge potential of our solutions to reduce the future huge energy demand related to factory automation.

Keywords: industrial internet of things (IIoT); non-orthogonal multiple access (NOMA); energy efficiency; power splitting (PS); simultaneous wireless information and power transfer (SWIPT); factory of the future

1. Introduction

Every year, the number of Internet-enabled gadgets grows. By 2025, 30 billion connected devices are expected to exist, which means that bandwidth, reliability, and latency demands will rise accordingly [1,2]. The Industrial Internet of Things (IIoT) is a term that will be used to describe these connected gadgets in the future. As illustrated in Figure 1, the IIoT is rapidly evolving and spans several industries and services. Co-channel interference, connection failures, and long end-to-end delays are all potential problems with these devices, but their short battery life is the most difficult to overcome [2]. A city-wide communication network will need advanced power distribution algorithms, due to environmental concerns and the high expense of battery management/replacement. These

strategies would help IIoT devices with low power, and they would also make it easier for people to talk to each other in a smart city [3,4].
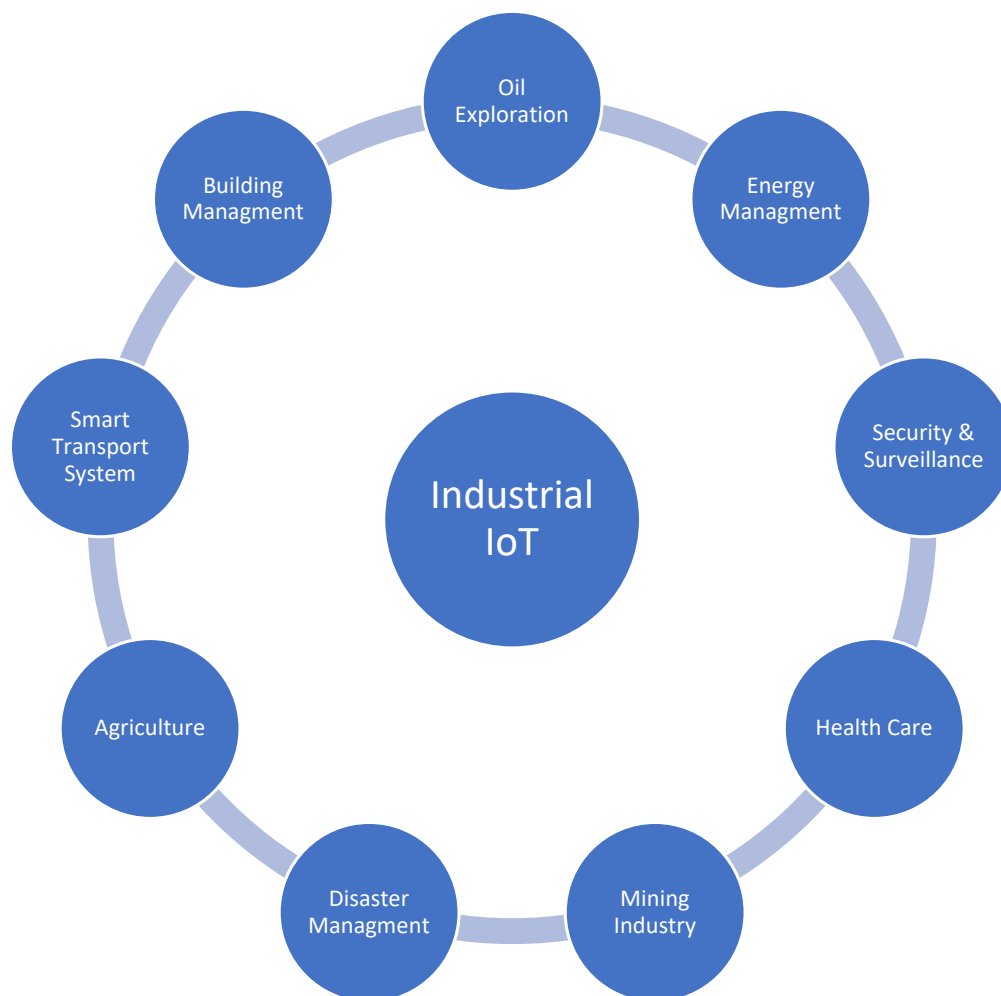

Figure 1. Major businesses and services that use IIoT [3].

The 5G and 6G communication systems will require high spectral efficiency [5] to set the path for the future IIoT era, which aspires to ultra-reliable low-latency communications and massive machine-type communication (mMTC). Non-orthogonal multiple access (NOMA) has become a viable option for IIoT systems owing to its better spectral efficiency performance [6,7]. This is because standard orthogonal multiple access (OMA) techniques are unable to fulfill the need for greater SE. The orthogonal multiple access (OMA) approaches have been widely adopted, where restricted resources, such as spectrum resources, sub-channels, and resource blocks, are assigned to each user. To a limited extent, they can reduce the impact of interfering signals in vast and substantial IIoT networks. However, this does not scale up as the number of IIoT equipment grows. The number of end users is growing quickly, so future smart cities will need access methods that are both scalable and efficient with spectrum [8].

The effectiveness of the suggested strategy is emphasized through extensive simulations, highlighting that the proposed technique greatly outperforms the unsatisfactory NOMA scheme for IIoT devices. The following are the primary contributions of this work.

We consider a SWIPT NOMA-enabled IIoT network, in which a single base station (BS) supports N IIoT devices, in a future autonomous factory through M sub-channels for each device, as shown in Figure 2. A unique optimum power allocation technique has been developed to increase the overall EE of IIoT devices.
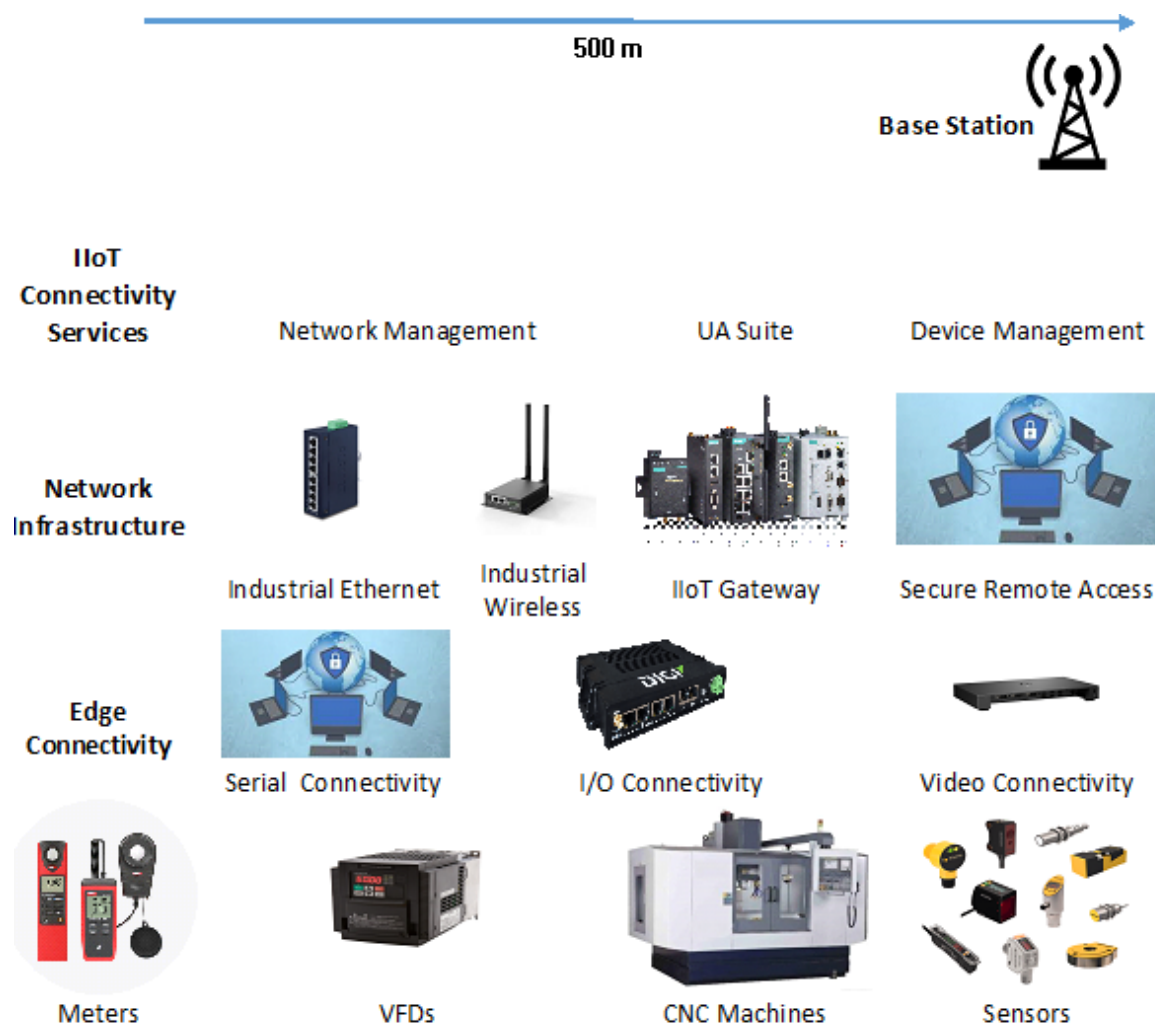
Figure 2. Wireless factory automation of IIoT devices.

We used a multi-objective model for a SWIPT NOMA-enabled IIoT network with the purpose of simultaneously maximizing total harvested energy and total transmission rate. Using the Shannon formula, we translate the gathered energy into throughput. The analyzed MOO model is, then, turned into a single-objective model using the scalarization method. The associated non-convex issue entails joint optimization of power allocation and splitting control; hence, we propose decoupling the problem into two sub-problems and solving them using the Lagrangian duality technique. Numerical results show that applying the proposed methods in the factory of the future provides considerable performance gains in energy efficiency.

The remainder of this work is structured as follows. Section 2 briefly offers some background information and literature review. Section 3 outlines our contributions. Section 4 briefly explains the research directions in energy IIoT systems for the factory of the future. Section 5 describes the system model and the problem formulation. Section 6 introduces the derivation of the SWIPT-NOMA System. The simulation results are reported in Section 7, and the conclusions are presented in Section 8. Throughout the paper, Scalar and vector are represented by non-bold and bold case characters, respectively.

2. Literature Review

Cellular traffic now employs OMA mechanisms for devices to connect to the Internet, which is common practice. Using NOMA approaches can aid in the provision of services such as massive machine-type communications (mMTC) and ultra-reliable low latency

communications (URLLC) [9,10]. After the development of (IIoT) devices, mobile traffic will occupy a significant chunk of the spectrum. As a result, the use of NOMA approaches for bandwidth and resource distribution becomes even more critical [11,12]. With NOMA, non-orthogonality is usually achieved by power domain modifications. Through the power domain, transmitted data can be multiplexed in frequency, time, and code domains [13].

In contrast to OMA, the primary notion of NOMA is to serve numerous IIoT devices in the same resource block. This enhances SE [14] by taking advantage of the recourse gain difference, which allows multiple users to be scheduled on a single spectrum resource. With user fairness in mind, NOMA systems outperform OMA systems in terms of optimum sum rate performance. The authors demonstrated and explored the advantages of NOMA over OMA in actual Rayleigh fading channels. To make things more feasible, the authors in [15] examined dynamic traffic arrival, for geographically random users, in the downlink NOMA transmission system. They demonstrated that the suggested NOMA technique yields bigger stable throughput zones than OMA, utilizing tools from queueing theory and stochastic geometry [16]. NOMA research has also been expanded to include systems with multiple inputs and outputs (MIMO) [17], millimeter-wave communications (mmWave) [18], and mobile edge computing (MEC) [19].

An end-to-end detection technique for multiple users can then be utilized at the receiver, e.g., successive interference cancelation (SIC) [20]. As a result, the same spectrum may be utilized at both the transmitter and reception ends, thanks to superposition-coding at the former and SIC at the latter [21]. To put it simply, this occurs because the receiver initially decodes the strongest users first and regards the others as noise and interference. After that, the strongest signal is removed. There is no end in sight to this process of removing unintended/interference messages [22]. One can also say that the innovative aspect of NOMA is intelligently allocating transmitting power to various IIoT devices. This becomes much more crucial in the case of low-powered micro IIoT devices with limited energy sources.

Meanwhile, energy efficiency (EE) strategies have been studied in a traditional NOMA system [23]. The authors of [24] presented a multi-user downlink NOMA approach. They covered several applications of coordinated multipoint NOMA algorithms for signal downlink transmission. The authors of [25] employed Alamouti codes. Their goal was to deliver a decent data rate for the edge user without sacrificing the near user. They presented a group-based approach for edge users [26]. As a result, they present a closed-form solution, for outage probability in an opportunistic NOMA system, with power optimization for multi-cell users. Similarly, the authors of [27] offered a poor scheduling technique, whereas the authors of [20] used the relaying signal to distribute power among several cells. The authors of [28] addressed the topic of dynamic power regulation in order to increase the cumulative capacity of consumers while reducing total transmission power. Additionally, they investigated a communication environment in which NOMA users form two-user groups.

The authors of [29] explored resource management issues in multi-cell MIMO systems. In [30], the authors presented a suboptimal approach to optimize the cumulative capacity of the users. Their findings show that even adopting inferior procedures may result in considerable increases in NOMA system user capacity. The authors of [31] evaluated outage probability, EE, and system effective capacity. Similarly, the authors in [32] offered a suboptimal strategy for dealing with the non-convex optimization issue. The authors of [33] also investigated the difficulty of managing resources in heterogeneous communication networks based on NOMA.

In [34], the authors presented an efficient power allocation method to optimize the EE of small cells. They derived an efficient solution using a closed-form expression. Authors in [35] investigated the power distribution and the sub-channel assignment to increase the EE of small cells. They presented a new suboptimal strategy of dual decomposition.

EE approaches in NOMA-enabled IIoT networks were also investigated. The dynamic user scheduling and power control in IIoT networks, for example, were examined by the au-

thors [36]. The task was given as a stochastic optimization with the purpose of minimizing network power consumption. Using a branch and bound technique, the authors found the most efficient power allocation in [37]. They investigated an efficient resource management challenge to optimize the energy efficiency of a NOMA-enabled IIoT system based on energy harvesting. In [38], the authors presented an effective approach to identify the optimal solution using a mesh adaptive direct search. Moreover, wirelessly powered IIoT networks, supported by power domain NOMA, are described in [38]. The authors of [39] investigated the problem of resource allocation for EE, using nonlinear energy harvesting, in machine-to-machine communication. The objective was to reduce total network power consumption by integrating transmit power and temporal resource management. To arrive at an efficient solution, the authors altered the problem before employing a strategy for efficient time allocation and power control in [40]. They first created an efficient technique for combining time allocation and rate allocation task offloading for a specific task edge-server.

The authors of [41] improved the mMTC system's energy efficiency by combining resource management with computation resources. They made a closed-form formula for suboptimal power control and used matching theory to make sure that sub-channels were given to the right people.

Nevertheless, to address the requirement for high data rate services, 5G application possibilities, including blockchain-based IIoT ecosystems and smart cities, require long-life batteries [42]. Recent developments in wireless power transfer research indicate that the lifetime of energy-constrained wireless devices may be increased [43]. Furthermore, since radio frequency (RF) signals may transport both information and energy, wireless power transfer and wireless information transfer can be integrated into communication networks. Therefore, simultaneous wireless information and power transfer (SWIPT) has recently evolved with the objective of accomplishing simultaneous information and energy transmission. However, the authors in [44] conducted the first information-theoretic investigation into SWIPT. Despite being insightful, present energy harvesting devices are not yet capable of directly decoding the transported information since the sensitivity of receivers differs substantially, so theoretical restrictions of this kind are not feasible. As a result, two new receiver structures, the time-switching (TS) scheme and the power-splitting (PS) scheme, were created in which information decoding (ID) and energy harvesting (EH) were separated via the time domain and the power domain, respectively [44].

The authors of [45,46] suggested a power allocation-based SWIPT approach with independent splitting control, assuming that the digitally modulated subcarriers are segregated into two classes of ID and EH. They investigated the SWIPT method for a small-cell communication system, addressing the combined optimization of time scale ratios and spatial precoding to collect energy from all UEs [46]. They investigated the maximization of EH efficiency, in multi-cell MISO techniques, for both linear and non-linear systems. The SWIPT-enabled NOMA system has grabbed the interest of many because of its huge potential. In [47], the authors investigated the cooperative design of uplink information transmission and downlink energy transfer in a wireless-powered NOMA communication system. Two ways were proposed for improving operational fairness and individual optimization: "time sharing" and "fixed decoding order." The combination of SWIPT and NOMA suggested that system performance might be considerably improved. Given the vulnerability of wireless powered networks to the cascading near-far problem, the authors in [48] employed matching priority weights to optimize the downlink/uplink user rate. Furthermore, in the SWIPT-enabled NOMA system, the cooperative NOMA scheme was extensively adopted, with near-NOMA users near the source acting as energy harvesting sources to aid distant NOMA users with poor channel conditions. Additionally, an iterative optimization method was made to get the best possible sum rate in a NOMA mmWave massive MIMO system with SWIPT. Table 1 summarizes recent works on SWIPT-aided energy harvesting.

Table 1. Summary of recent works on SWIPT-aided energy harvesting.

Reference	Title	Focus	Limitations
[14] (Xu 2019)	Resource allocation in OFDM-based wireless powered communication networks with SWIPT	Propose a suboptimal resource allocation scheme to maximize the weighted downlink and uplink sum rate by optimizing the time, subcarrier and power allocation	Do not consider NOMA
[17] (Zhou 2019)	Secure SWIPT for Directional Modulation-Aided AF Relaying Networks	Formulate an optimization problem based on maximizing the signal-to-leakage-artificial-noise-ratio criterion, and transform it into a semidefinite relaxation (SDR) problem for amplify-and-forward relaying	Do not consider NOMA
[26] (Hu 2019)	SWIPT-enabled relaying in IoT networks operating with finite blocklength codes	Propose a power splitting (PS) and time switching (TS) protocol to improve SWIPT reliability, combined with blocklength allocation optimization between relaying hops	Do not consider NOMA
[31] (Jang 2018)	Energy efficient SWIPT systems in multi-cell MISO networks	Propose optimal beamforming methods based on the semidefinite relaxation (SDR) and the successive convex approximation (SCA) technique for multi-cell multi-user MISO SWIPT systems	Do not consider NOMA
[32] (Xiang 2018)	Energy efficiency for SWIPT in MIMO two-way amplify-and-forward relay networks	Propose joint sources and relay precoding matrices, and the PS ratio to maximize the EE of the network, under the transmit power constraints and the minimum SE requirement	Do not consider NOMA
[8] (Tran 2021)	SWIPT Model Adopting a PS Framework to Aid IoT Networks Inspired by the Emerging Cooperative NOMA Technique	Apply SWIPT considering power splitting (PS) factors to harvest energy for half-duplex and full-duplex relaying and combat eavesdroppers	Do not consider spectrum or energy efficiency as performance evaluation
[29] (Xu 2017)	Joint beamforming and power-splitting control in downlink cooperative SWIPT NOMA systems	Propose a cooperative SWIPT-aided NOMA using a golden section search (GSS) algorithm for a global optimal solution.	Do not consider spectral or energy efficiency as performance evaluation
[48] (Rauniyar 2021)	Ergodic sum capacity analysis of NOMA—SWIPT enabled IoT relay systems	Propose the use of IoT node for the dual role of relaying the source node data and offloading data to its own destination based on TS and PS relaying	Do not consider spectral efficiency as performance evaluation
[34] (Tang 2020)	Joint Power Allocation and Splitting Control for SWIPT-Enabled NOMA Systems	Propose a joint optimization on transmission rate and harvested energy to be solved using iterative convex subproblems	Do not consider specific IoT use case
[25] (Andrawes 2020)	Energy-Efficient Downlink for Non-Orthogonal Multiple Access with SWIPT under Constrained Throughput	Propose use of genetic algorithm to optimize power splitting ratio power allocation coefficients towards improving the outage probability	Do not consider specific IoT use case

3. Our Contributions

This paper sheds light on the power optimization framework for NOMA-enabled IIoT devices, which is motivated by the aforementioned advancements. The goal is to reduce the total transmitted power of IIoT devices and improve their energy efficiency. The combination of NOMA and SWIPT is envisioned as an enabling technology for the future 5G/6G network. As a result, jointly maximizing the total transmission rate and total captured energy in a SWIPT NOMA-enabled IoT network is presented. We use a multi-objective optimization (MOO) model for a SWIPT NOMA-enabled IIoT network, in which we investigate the most efficient resource allocation strategy by jointly optimizing power allocation and splitting control, all while meeting certain QoS requirements in terms of transmission rate and harvested energy. To tackle the non-convex power optimization problem for a specific sub-channel assignment, we use a novel technique based on the Langrangian duality method [48]. The effectiveness of the proposed strategy is emphasized through extensive simulations, highlighting that the proposed technique greatly outperforms the unsatisfactory NOMA scheme for IIoT devices. The following are the primary contributions of this work:

1. We consider a SWIPT NOMA-enabled IIoT network, in which a single base station (BS) supports N IIoT devices, in a future autonomous factory through M sub-channels. A unique optimum power allocation technique has been developed to increase the overall EE of IIoT devices. The problem is described with constraints such as the individual QoS requirements, the maximum transmitting power, and the minimum harvested energy for each IIoT device on each sub-channel.
2. We used a MOO model for a SWIPT NOMA-enabled IIoT system with the goal of maximizing both total transmission rate and total gathered energy at the same time. Next, we convert the harvested energy into throughput using the Shannon formula. Then, the examined MOO model is turned into a single-objective optimization (SOO) model by using the scalarization method.
3. The corresponding problem, which involves joint optimization of power allocation and splitting control, is still non-convex and, thus, we propose decoupling the problem into two sub-problems to solve them iteratively via the Langrangian duality method.

4. Research Directions in Energy IIOT Systems for Factory of the Future

In the past few years, smart manufacturing systems have advanced in many development domains to improve productivity and effectiveness, where intelligent manufacturing IIoT in a future autonomous factory, such as drones and manufacturing lines, interact with one another and with workers.

4.1. 5G Systems and Beyond

Various kinds of technological tools are collaborating to create conditions that foster exchange and intelligent features, which is speeding up the development of the intelligent Industrial Internet-of-Things (IIOT). This type of automation system is needed to handle enormous amounts of information and manage complex cyber–physical aspects, facilitating autonomous manufacturing. For precise instrument control, autonomous manufacturers, as well as crisis preparedness and prevention, a great proportion of sensing devices are helpful for gathering actual information for quick turnaround during the production process [49]. The 3GPP has identified the most important aspects of industrial automation, including automated testing, which necessitates telecommunications for monitoring, fully accessible system control, and processing remote monitoring functions within a manufacturing building. This demands a wide range of devices and processors [50]. Production automation technology needs incredibly low connectivity on the user's end, such as 10 ms E2E duration and (1–10) dependability. For the last several, typical confined movement management and remote surveillance applications, a much more extreme E2E duration of 1 ms is required, as well as more stringent dependability of (1–10–8) or above. In the same way, some of the

biggest problems with automobile IIoT have been identified, by the Clear 5G initiative, as requirements for maximum load capacity [51].

According to the Clear 5G objective, the biggest hurdles are resolving the lack of real-time control over a number of wireless internet services, including mobile network layout, throughout radio communication systems and frequency equilibrium. Industrial Internet of Things are also limited by issues such as how much power they can use and how much computing power they can have [52]. When complex computing tasks are done on mobile devices (MDs), their limited use cases could have a huge effect on QoS.

4.2. Mobile Edge Computing

By bringing system resources nearer to the equipment, the Mobile Edge Computing (MEC) innovation brings a different solution to these problems. The MEC scheme could also provide a quality service with a fast response time, high throughput, and network data storage. All of these features were made to fit a wide range of URLLC situations, such as real-time surveillance and software products, for industrial automation [53].

The Clear5G project is focused on the potential of a multi-RAT scenario to manage the enormous number of visitors at a sophisticated factory site. Companies are frequently using the unauthorized spectrum, in addition to the formal frequency, to minimize wireless demand on the formal frequency. Numerous novel unlicensed frequency techniques have converged and are now being researched, notably including LTE on Unauthorized, LTE Certified Accessibility, and LTE-WLAN Amplification [54]. The above access network innovations have led to the establishment of a new type of communication environment, which is essential to increasing wireless coverage and available bandwidth [55]. In recent years, the integration of 5G Different Broadcasting in Unapproved Spectral Range and MEC has emerged as a viable solution for meeting the demanding IIoT usage scenarios [56].

4.3. Mobile Device Description

An MD is furnished with just one—or maybe more—lenses that capture legitimate broadcasting for environmental control at the relevant factory of the future (FoF). MDs have the capacity to maintain a careful eye on their ability to respond appropriately based on what they observe [57]. Contrarily, unprocessed videos should be analyzed with computer vision applications to discover knowledge, including movie labels or object identification. Nevertheless, we suppose that the MDs seem unable to accomplish the duties through their own associated physical and mechanical limitations, so they would always transfer significant parts of the project to the internet [58]. GPU multitasking in the MEC or cloud platform can accelerate the video encoder due to the rapid advancement of learned in the classroom algorithms in the machine vision domain [59]. These important facts can be supplied in a comprehensive, continuing-to-learn integrated process that can decide things [60,61]

4.4. Industry 4.0

With the onset of Industry 4.0, the world is concentrating on combining ICT devices to increase efficiency [62]. Legislative intervention is being sought by countries all over the world to promote energy efficiency, while ICT companies are launching energy management solutions that employ big data to visualize and optimize energy flow and expenditure. The industrial sector needs the most electricity. Industrial electricity can reduce production costs even while improving productivity and increasing [63]. To minimize energy use, the production industry has adopted equipment energy conservation measures, including such things as upgrading elevated machinery. For this strategy to work, it needs an initial investment and a certain amount of time [64].

Since there is no framework for integrative modelling within a company and constant monitoring of electricity consumption, just as there is with conventional electricity grids at the unit level, facility conditions are segregated and cannot be fully understood. From this insufficient information, implementing electricity decisions in real time is difficult.

Manufacturing power consciousness or management can, indeed, be improved significantly by evaluating power consumption information online and integrating energy optimization into current control. Internet access, which is commonly used in modern work, may be able to help the optimization succeed [65,66].

4.5. Raising Energy Awareness

In the foreseeable future, the Fuel-Efficient Factories of the Future will function by consistently collecting power rich data from any selected area on the production line and combining it with organization data for business's ability management. The inside glimpse at power consumption is being shown.

In this circumstance, pervasive computing equipment can also be used in combination with smart monitoring approaches to constantly monitor information, irrespective of where all the origins are sited, and then convert it into company insights. The information will be expanded and displayed to provide electricity automated scheduled maintenance, electricity item/network duration management (for ongoing traceability devices), and appropriate timing and equilibrium of manufacturing production lines.

At an industry scale, power generation consciousness will be applied via computer network techniques that enable automatic detection of sensing devices, RFID readers, laptops, smart applications, and PLCs, as well as on and in-network data analysis. Conventional monitoring equipment will be improved with the ability to interpret original information, retrieve company knowledge at the origin, as well as provide internet resources, reducing the necessity for a unified software package to extract information. Collection of property data points will be facilitated by mobile and interior location-specific devices [67].

Furthermore, as presented in Figure 3, fuel efficiency goes beyond simple surveillance and hold ruling procedures at the community scale. Interaction is very important throughout multiple sectors, such as the manufacturer, the financial world, including business applications, and even building automation. Information from all levels must be connected and reviewed to contribute to a fuel efficient strategy that takes a holistic view of how energy consumption can be accomplished. Cross-enterprise concerns, such as transportation for transporting supplies and materials before and after manufacturing, should also be addressed. In addition, external organizations, including a smarter power grid and better aggregation of information, will be needed to pass the strategy.
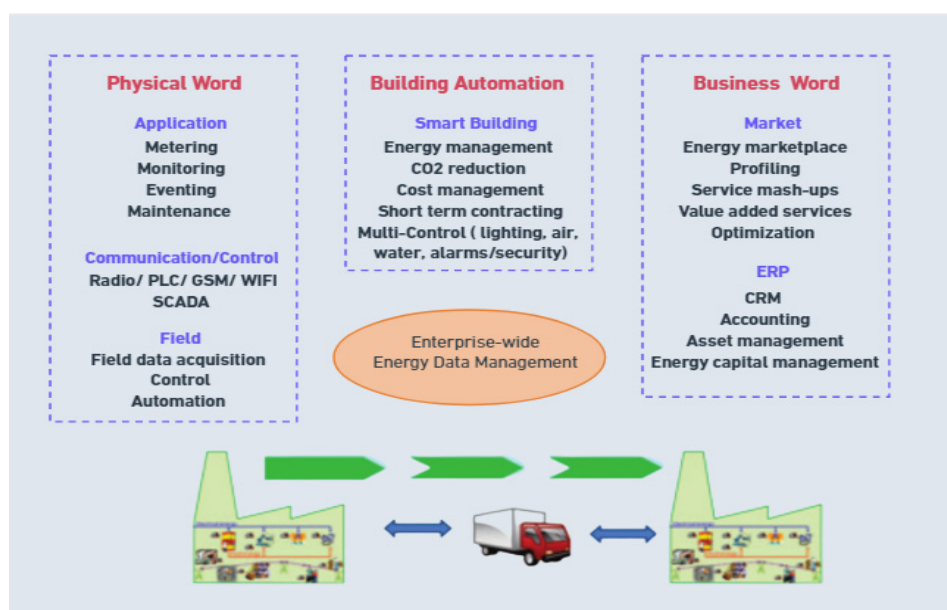

Figure 3. Cross-Enterprise Energy Efficiency for Factory of the Future.

The efficient use of energy at the site level requires flexible resource and operation administration. There will be a price consideration in processes, assembly, distribution efficiency, as well as electricity indicators. To guarantee comprehensive management and oversight, efficiency cycles will be established at all stages of manufacturing, from the industrial automation to the Enterprise Resource Planning (ERP). Management choices can be taken with full understanding of the energy demand situation on the production line by using this closed loop approach. WebSocket, for portable systems and autonomous asset identification, will be developed to ensure tunability and connectivity from of the hardware level up to ERP [68].

Conventional methods for collecting and interpreting information, obtained from the production floor, employ handmade platforms. The information is managed and graphically represented so that individuals can comprehend it. Employees must have a strong grasp of the facility (systems, manufacturing structure, etc.) and industrial automation experience in addition to understanding the condition of the process. Employing statistical analysis to make data-driven decisions (e.g., Six Sigma) has shown productivity improvements of 40–60% in actual case scenarios [69].

5. System Model and Problem Formulation

In this section, an Industrial IoT (IIoT) system network is studied in which a single base station (BS) serves N IIoT devices through M sub-channels. This form of communication can occur among different IIoT devices that are connected to an RF transmission source in general. We investigate the NOMA system model based on SWIPT. Then, we derive and mathematically formulate the optimization problem. A downlink NOMA system with a single base station (BS) and N IIoT devices is taken into consideration. We assume that all terminals have complete knowledge of the channel state information (CSI). You can get downlink CSI from pilots, and uplink channel estimate in TDD mode can give you transmitter-side channel estimation, which can be used to get receiver-side channel estimation. It is possible to rank channel gains as $|h_{1,m}|^2 < |h_{2,m}|^2 < \ldots < |h_{n,m}|^2$ without losing generality by using the notation $|h_{n,m}|^2$ to represent the channel power gain for sub-channel $m \in M$. If S_m represents the set of IIoT devices on sub-channel $m \in M$, IIoT devices' messages are superimposed by allocating distinct powers, which is represented as $p_{l,m}$ for IIoT device $l \in S_m$ in NOMA system [29]. In this way, the transmit signal $x_{l,m}$ on sub-channel m can be described as follows [7,8,33,48]:

$$x_{l,m} = \sum_{m=1}^{M} \sum_{l=1}^{S_m} \sqrt{p_{l,m}} x_{l,m} \tag{1}$$

where $x_{l,m}$ is the message for IIoT device l on sub-channel m. We have the following constraint since the overall power of BS is restricted

$$\sum_{m=1}^{M} \sum_{l=1}^{S_m} \sqrt{p_{l,m}} \leq P_T, \tag{2}$$

where P_T denotes the total transmission power available at the BS.

We implement SWIPT through using the power splitting (PS) approach, assuming that all IIoT devices are capable of harvesting energy through RF signals. Consequently, to simultaneously use EH and ID, receivers with a signal processing module and a harvested energy module are being investigated in this study. To maximize energy harvesting and information transmission, the BS signals are divided into two segments using the PS approach. Let us assume that $\rho_l \, \forall \, 0 \leq \rho_l \leq 1$, and ρ_l denotes the proportion of transmission power assigned to IIoT device l for ID. Additionally, $(1 - \rho_l)$ is the proportion of transmis-

sion power assigned to IIoT device l for EH. In this configuration, the signal received by IIoT device l's sub-channel m ID receiver is

$$y_{l,m}^{ID} = h_{l,m}\sqrt{\rho_l}x_{l,m} + n_{l,m}, \tag{3}$$

where $n_{l,m}$ is the independent zero-mean additive white Gaussian noise (AWGN) with variance (σ^2). For any $i > j$, each device u_i will be able to detect and eliminate the message of u_j from its received signal via successive interference cancellation (SIC). In the case $i < j$, the message of device u_j will be ignored [30]. In terms of feasible transmission rates for device l on sub-channel m, we can use the following formula as follows:

$$R_{l,m}^{ID} = log_2\left(1 + \frac{\rho_l|h_{l,m}|^2 p_{l,m}}{\rho_l|h_{l,m}|^2 \sum_{i=1}^{S_m} p_{i,m} + \sigma^2}\right). \tag{4}$$

Then, one can express the transmission rate as follows:

$$R_{ID} = \sum_{m=1}^{M}\sum_{l=1}^{S_m} R_{l,m}^{ID}. \tag{5}$$

For EH, the received signal of device l is defined as

$$y_{l,m}^{EH} = \sqrt{1 - \rho_l}x_{l,m}h_{l,m} + n_{l,m}, \tag{6}$$

Here, we explore a well-recognized linear EH model [16–25]. This assumption is suitable because the amount of harvested energy is often little in reality, as illustrated by [20], which demonstrates that, by appropriately adjusting the energy conversion efficiency, it is feasible to adapt the linear EH framework to the non-linear EH theory at weak power input. Furthermore, since we consider total harvested energy to be one of our optimization objectives in the provided system, we may conclude that collected energy somehow doesn't exceed the receiver saturated criteria. Consequently, the captured energy at the receiver of device l is provided by:

$$e_{l,m} = \eta(1 - \rho_l)|h_{l,m}|^2 p_{l,m}, \tag{7}$$

where η denotes the efficiency of energy conversion. We also assume that the noise is far less and, hence, insignificant. The system's total harvested energy can be expressed as

$$E = \sum_{m=1}^{M}\sum_{l=1}^{S_m} e_{l,m}, \tag{8}$$

In this paper, our goal is to optimize both the entire amount of energy harvested and the overall transmission rate. One can write the optimization problem with the minimal transmission rate objectives, the minimal transmitted energy requirements, and the overall power limit in consideration. Let us assume that each device's QoS constraints are similar. However, one can formally write the optimization problem as:

$$P1: \max_{\{p_{l,m}\},\{\rho_n\}}\left\{R_{ID}(p_{l,m},\rho_l), E(p_{l,m},\rho_l)\right\} \tag{9}$$

$$s.t. \quad \sum_{m=1}^{M}\sum_{l=1}^{S_m} p_{l,m} \leq P_T, \tag{9a}$$

$$R_{l,m}^{ID} \geq R_{min}, \; \forall\, l, m, \tag{9b}$$

$$e_{l,m} \geq E_{min}, \; \forall\, l, m, \tag{9c}$$

$$0 \leq \rho_l \leq 1 \quad \forall\, l \tag{9d}$$

$$p_{l,m} \geq 0 \quad \forall\, l \tag{9e}$$

The constraint (9a) indicates that the aggregate of transmitted power for all devices never surpasses the P_T threshold, which is the BS's maximum power. Constraint (9b) meets the lth devices's QoS requirement. Constraint (9c) indicates that each lth device is required to harvest at least the minimum harvested energy E_{min} for each lth device. The constraint (9d) requires that the power splitting factor ρ_l of the lth device be between [0,1]. The constraint (9e) implies that the power allocated of the lth device is non-negative.

The optimization problem (P1) is a widely known Multi-Objective Optimization (MOO) problem [31–33]. According to [33], the problem P1 can be turned into a Single Objective Optimization (SOO) problem.

Nevertheless, because the unit for $R_{l,m}^{ID}$ is bit/s/Hz, which is different than the unit of E in Watts, it is not suitable to sum them directly. To align the units of these two cost objectives, we use the Shannon formula to translate the harvested energy into throughput, and then, we establish a unique performance metric by adding the weighted constants of the transmission rate attained by information decoding and the transformed throughput from energy harvested [33].

In this section, we define $R_{l,m}^{EH}$ to represent the feasible rate that is changed from device l's harvested energy as follows:

$$R_{l,m}^{EH} = log_2\left(1 + \frac{\gamma\eta(1-\rho_l)|h_{l,m}|^2 \sum_{m=1}^{M}\sum_{l=1}^{S_m} p_{l,m}}{\sigma^2}\right). \tag{10}$$

where γ represents the efficiency of transferring battery power to RF power. Then, one can express the transmission rate from EH as follows:

$$R_{EH} = \sum_{m=1}^{M}\sum_{l=1}^{S_m} R_{l,m}^{EH}. \tag{11}$$

Then, the cost function of the new optimization problem is given as

$$R = aR_{ID} + bR_{EH} \tag{12}$$

where a and b denote non-negative rating numbers for both cost functions. However, R represents the total of the information decoding rate and the harvested energy. To make things easier, we will normalize a as 1 and $\tau = \frac{a}{b}$. As a result, the objective function is recast as follows:

$$R = R_{ID} + \tau R_{EH} \tag{13}$$

where τ represent the weight used to govern the precedence of service between ID and EH.

According to the Equations (5), (11), and (13), the objective function of the data rate of device l on sub-channel m is given as follows:

$$R = \sum_{m=1}^{M}\sum_{l=1}^{S_m} log_2\left(1 + \frac{\rho_l|h_{l,m}|^2 p_{l,m}}{\rho_l|h_{l,m}|^2 \sum_{i=1}^{S_m} p_{i,m} + \sigma^2}\right) + \tau\sum_{m=1}^{M}\sum_{l=1}^{S_m} log_2\left(1 + \frac{\gamma\eta(1-\rho_l)|h_{l,m}|^2 \sum_{m=1}^{M}\sum_{l=1}^{S_m} p_{l,m}}{\sigma^2}\right) \tag{14}$$

As a consequence, one can rewrite the problem in (14) as:

$$P2: \max_{\{p_{l,m}\},\{\rho_l\}} \left\{R(p_{l,m}, \rho_l)\right\} \tag{15}$$

$$s.t. \sum_{m=1}^{M}\sum_{l=1}^{S_m} p_{l,m} \leq P_T, \tag{15a}$$

$$R_{l,m}^{ID} \geq R_{min}, \ \forall\, l, m, \tag{15b}$$

$$e_{l,m} \geq E_{min}, \ \forall\, l, m, \tag{15c}$$

$$0 \leq \rho_l \leq 1 \quad \forall\, l \tag{15d}$$

$$p_{l,m} \geq 0 \quad \forall\, l, m \tag{15e}$$

The problem in (15) is joint non-convex optimization, with splitting control and power allocation in the existence of device entanglement. Nevertheless, an exhaustive search strategy across all conceivable PS ratio and power allocation combinations can be used. To that end, because of the coupling of several variables and the existence of inter-user interference, the problem presented in (15) is neither convex nor linear [57]. Furthermore, as mentioned in [70], for any optimization issue with multiple variables, we may analyze and solve the problem over certain variables while treating the others as constants, and then solve the problem over the remaining variables.

6. Derivation of the SWIPT-NOMA System

We examined the joint optimization in SWIPT NOMA-enabled IIoT systems in (15) to find the greatest achievable rate. Equations in (15) are non-convex optimizations. Therefore, finding optimum solutions is quite tough. An iterative optimization method is developed to handle this intractable problem. We divide the problem in (15) into two suboptimal problems while meeting the desired EH limitations and transmit power constraint requirements.

Nonetheless, this comprehensive search approach incurs significant processing expense as the number of devices increases. To overcome this problem, we devise an iterative strategy based on the Lagrangian duality methodology [48,70], as shown below. According to [70], for any optimization problem with various variables, it is possible to deal with the sub-problem over a subset of variables while treating the other variables as constants before, then, pivoting to deal with the sub-problem over the remaining variables. Consequently, $p_{l,m}$ and ρ_l are separated to construct a realistic and efficient solution for the examined optimization problem in (15).

Firstly, one can consider the case where the power allocation is $(p_{l,m} \; \forall \; l, m) \in Constant$. In this section, we concentrate on maximizing the power splits variables $\rho_l \forall \; l$, given constant power allocations $p_{l,m} \; \forall \; l, m$. The optimization sub-problem, on the other hand, can be reformulated as described in the following:

$$P3: \quad \max_{\boldsymbol{\rho}} \{R(\boldsymbol{\rho})\} \tag{16}$$

$$s.t. \quad R_{l,m}^{ID} \geq R_{min}, \; \forall \; l, m, \tag{16a}$$

$$e_{l,m} \geq E_{min}, \; \forall \; l, m, \tag{16b}$$

$$0 \leq \rho_l \leq 1 \quad \forall \; l \tag{16c}$$

According to (14) and Constraints (16a), (16b), and (16c), $\rho_l \; \forall \; l$ is required to satisfy the following condition

$$\rho_l^{Lower} \cong \frac{(2^{R_{min}} - 1)\sigma^2}{|h_{l,m}|^2 p_{l,m} - (2^{R_{min}} - 1)|h_{l,m}|^2 \sum_{i=l+1}^{S_m} p_{i,m}} \leq \rho_n \leq 1 - \frac{E_{min}}{|h_{n,m}|^2 \sum_{m=1}^{M} \sum_{l=1}^{S_m} p_{l,m}} \cong \rho_l^{upper}, \tag{17}$$

Considering (16c) and (17) united, the considered problem becomes infeasible only if $\rho_l^{lower} > 0 \; \forall \; l$ and $\rho_l^{upper} > 0 \; \forall \; l$.

Based on the result in [48,49], the problem in (16) is a convex optimization for the power splitting factors $\rho_l \; \forall \; l$. To certify the convexity of the optimization problem in (16), we initially make sure that the power splitting parameter domain is quasi and convex. Due to the constraint of $\rho_l^{lower} > 0 \; \forall \; l$ and $\rho_l^{upper} > 0 \; \forall \; l$, the possible range of the power splitting factor is quasi. One can also find the convexity due to the Equations (16a), (16b), and (17). In (16), the objective function is shown to be concave on the power-splitting variables $\rho_l \; \forall \; l$.

Assume that the achievable data rate for device l on sub-channel m is

$$R_g = log_2\left(1 + \frac{\rho_l |h_{l,m}|^2 p_{l,m}}{\rho_l |h_{l,m}|^2 \sum_{i=l+1}^{S_m} p_{i,m} + \sigma^2}\right) + \tau log_2\left(1 + \frac{\gamma\eta(1 - \rho_l)|h_{l,m}|^2 \sum_{m=1}^{M} \sum_{l=1}^{S_m} p_{l,m}}{\sigma^2}\right) \tag{18}$$

Thus, the first derivative of $R_{l,m}$ with respect to ρ_l is written as

$$\frac{\partial R_g(\rho_l)}{\partial \rho_l} = \frac{1}{ln2} \cdot \left(\frac{|h_{l,m}|^2 p_{l,m}\sigma^2}{\left(\rho_l|h_{l,m}|^2 \sum_{i=l+1}^{S_m} p_{i,m} + \sigma^2\right)\left(\rho_l|h_{l,m}|^2 \sum_{i=l+1}^{S_m} p_{i,m} + \sigma^2\right)} - \frac{\tau\gamma\eta|h_{l,m}|^2 P_T}{\gamma\eta(1-\rho_l)|h_{l,m}|^2 P_T + \sigma^2} \right) \tag{19}$$

Moreover, the second derivative of R_g, with respect to ρ_l, is expressed as

$$\frac{\partial^2 R_g}{\partial \rho_l^2} = -\frac{1}{ln2} \cdot \left(\frac{2\rho_l|h_{l,m}|^2 p_{l,m} \sum_{i=l+1}^{S_m} p_{i,m} \sum_{i=l+1}^{S_m} p_{i,m}\sigma^2 + |h_{l,m}|^4 p_{l,m}\left(\sum_{i=l+1}^{S_m} p_{i,m} + \sum_{i=l+1}^{S_m} p_{i,m}\right)\sigma^4}{\left(\rho_l|h_{l,m}|^2 \sum_{i=l+1}^{S_m} p_{i,m} + \sigma^2\right)^2 \left(\rho_l|h_{l,m}|^2 \sum_{i=l+1}^{S_m} p_{i,m} + \sigma^2\right)^2} \right)$$
$$- \frac{\tau\gamma^2\eta^2|h_{l,m}|^4 P_T^2}{\left(\gamma\eta(1-\rho_l)|h_{l,m}|^2 P_T + \sigma^2\right)^2} \tag{20}$$

And

$$\frac{\partial^2 R_g}{\partial \rho_i \partial \rho_j} = 0 \quad \forall i \neq j \tag{21}$$

According to (20) and (21), the Hessian matrix H is expressed as

$$H = \begin{pmatrix} H_1 & \cdots & 0 \\ \vdots & \ddots & \vdots \\ 0 & \cdots & H_{S_m} \end{pmatrix} \tag{22}$$

where $H_n = \frac{\partial^2 R_g}{\partial \rho_l^2} \leq 0$, $\forall l$. To put it another way, if the R g is concave, then the Hessian matrix is in the negative or equals zero range for all values of ρ_l $\forall l$. Due to its nature as a bounded aggregation from concave curves, objective function in (16) is inherently concave with respect to power splitting variables ρ_l, $\forall l$. To this purpose, the Lagrangian duality-based technique [33] can be used to achieve the closest solution to the optimization issue in (16). According to the formula, the Lagrangian function can be expressed as described in the following:

$$\begin{aligned}
\mathbf{Y}(\rho, v, \pi, \lambda, \mu) =\ & \sum_{m=1}^{M} \sum_{l=1}^{S_m} log_2\left(1 + \frac{\rho_l|h_{l,m}|^2 p_{l,m}}{\rho_l|h_{l,m}|^2 \sum_{i=l+1}^{S_m} p_i + \sigma^2}\right) \\
& + \tau \sum_{m=1}^{M} \sum_{l=1}^{S_m} log_2\left(1 + \frac{\gamma\eta(1-\rho_l)|h_{l,m}|^2 \sum_{m=1}^{M} \sum_{l=1}^{S_m} p_{l,m}}{\sigma^2}\right) \\
& + \sum_{l=1}^{S_m} v_l\left(R_{min} - \sum_{m=1}^{M} \sum_{l=1}^{S_m} log_2\left(1 + \frac{\rho_l|h_{l,m}|^2 p_{l,m}}{\rho_l|h_{l,m}|^2 \sum_{i=l+1}^{S_m} p_{i,m} + \sigma^2}\right)\right) \\
& + \sum_{l=1}^{S_m} \pi_l\left(\sum_{m=1}^{M} \sum_{l=1}^{S_m} log_2\left(1 + \frac{\gamma E_{min}}{\sigma^2}\right) - \sum_{m=1}^{M} \sum_{l=1}^{S_m} log_2\left(1 + \frac{\gamma\eta(1-\rho_l)|h_{l,m}|^2 \sum_{m=1}^{M} \sum_{l=1}^{S_m} p_{l,m}}{\sigma^2}\right)\right) \\
& + \sum_{l=1}^{S_m} \lambda_l \rho_l + \sum_{l=1}^{S_m} \mu_l(1-\rho_l)
\end{aligned} \tag{23}$$

where $v = [v_1, v_2, \ldots, v_{S_m}]^T$ and $\pi = [\pi_1, \pi_2, \ldots, \pi_{S_m}]^T$ are non-negative Lagrange multipliers, and they are corresponding to the constraint (16a) and the constraint (16b), respectively. $\lambda = [\lambda_1, \lambda_2, \ldots, \lambda_{S_m}]^T$ and $\mu = [\mu_1, \mu_2, \ldots, \mu_{S_m}]^T$ are non-negative Lagrange multipliers, and they are corresponding to the constraint (16c).

As a result, the Lagrange dual mathematical formulation can be expressed in terms of

$$\Gamma(v, \pi, \lambda, \mu) = \max_{\rho} \mathbf{Y}(\rho, v, \pi, \lambda, \mu) \tag{24}$$

The Lagrange dual optimization approach may, therefore, be outlined:

$$\min_{v, \pi, \lambda, \mu} \Gamma(v, \pi, \lambda, \mu) \tag{25}$$

$$s.t. \quad v \succcurlyeq 0, \pi \succcurlyeq 0, \lambda \succcurlyeq 0, \mu \succcurlyeq 0, \tag{26}$$

This Lagrange dual issue may be solved using the gradient descent technique and the sub-gradient strategy to adjust the dual parameters (v, π, λ, μ) with an optimal PS factor ρ. To maximize ρ_l for the given variables (v, π, λ, μ), we must identify the gradient direction of the Lagrange optimization method in Equation (23), as described in the following:

$$
\begin{aligned}
\nabla_{\rho_l} \mathbf{Y} = \frac{1}{ln2} \cdot \Bigg(& \frac{|h_{l,m}|^2 p_{l,m} \sigma^2}{\left(\rho_l |h_{l,m}|^2 \sum_{i=l+1}^{Sm} p_{i,m} + \sigma^2\right)\left(\rho_l |h_{l,m}|^2 \sum_{i=1}^{Sm} p_{i,m} + \sigma^2\right)} - \frac{\tau \gamma \eta |h_{l,m}|^2 P_T}{\gamma \eta (1-\rho_l)|h_{l,m}|^2 P_T + \sigma^2} \Bigg) \\
& - v_l \left(\frac{|h_{l,m}|^2 p_{l,m} \sigma^2}{ln2 \left(\rho_l |h_{l,m}|^2 \sum_{i=l+1}^{Sm} p_{i,m} + \sigma^2\right)\left(\rho_l |h_{l,m}|^2 \sum_{i=l+1}^{Sm} p_{i,m} + \sigma^2\right)} \right) \\
& - \pi_l \left(\frac{\tau \gamma \eta |h_{l,m}|^2 P_T}{ln2 \gamma \eta (1-\rho_l)|h_{l,m}|^2 P_T + \sigma^2} \right) + \lambda_l - \mu_l
\end{aligned}
\tag{27}
$$

Particularly, one can update the ρ_l as follows:

$$
\rho_l(Itr + 1) = \rho_l(Itr) + \varepsilon(Itr) \nabla_{\rho_l(Itr)} \mathbf{Y}
\tag{28}
$$

where $\rho_l(Itr)$ and $\rho_l(Itr + 1)$ represents the ρ_l in terms of Itr-th and $(Itr + 1)$-th iteration. $\varepsilon(Itr)$ represents step size of the ρ_l for Itr-th iteration to satisfy the condition as follows:

$$
\varepsilon(Itr) = arg \max_{\varepsilon} \mathbf{Y}(\boldsymbol{\rho}(Itr + 1), v, \pi, \lambda, \mu) \Big|_{\rho_l(Itr+1)=\rho_l(Itr)+\varepsilon(Itr)\nabla_{\rho_l(Itr)} \mathbf{Y}}
\tag{29}
$$

One can repeat the process in (28) until $\left| \nabla_{\rho_l(Itr)} \mathbf{Y} \right| \leq \epsilon_1 \ \forall \ l$. The $\boldsymbol{\rho}^*$ denotes the optimal power splitting factor. Therefore, one can rewrite the equation in (25) as follows:

$$
\Gamma(\lambda, \mu, v) = \mathbf{Y}(\boldsymbol{\rho}^*, v, \pi, \lambda, \mu)
\tag{30}
$$

Lagrange multipliers (v, π, λ, μ) are adjusted and computed after solving Equations (25) and (26).

On the subset of Lagrangian (v, π, λ, μ), the problem in (25) and (26) is clearly convex. As a result, optimizing the dual variables (v, π, λ, μ) may be solved using a 1-d heuristic approach. Although the desired function in (25) is often un-differentiable, this gradient-based technique is often impossible. When this isn't an option, we utilize the commonly used sub-gradient approach to calculate and determine the variables of (v, π, λ, μ).

$$
\nabla_{\lambda_l} \Gamma = \rho_l^*
\tag{31}
$$

$$
\nabla_{\mu_l} \Gamma = 1 - \rho_l^*
\tag{32}
$$

$$
\nabla_{v_l} \Gamma = R_{min} - \sum_{m=1}^{M} \sum_{l=1}^{Sm} log_2 \left(1 + \frac{\rho_l |h_{l,m}|^2 p_{l,m}}{\rho_l |h_{l,m}|^2 \sum_{i=l+1}^{Sm} p_{i,m} + \sigma^2} \right)
\tag{33}
$$

$$
\nabla_{\pi_l} \Gamma = \sum_{m=1}^{M} \sum_{l=1}^{Sm} log_2 \left(1 + \frac{\gamma E_{min}}{\sigma^2} \right) - \sum_{m=1}^{M} \sum_{l=1}^{Sm} log_2 \left(1 + \frac{\gamma \eta (1 - \rho_l)|h_{l,m}|^2 \sum_{m=1}^{M} \sum_{l=1}^{Sm} p_{l,m}}{\sigma^2} \right)
\tag{34}
$$

If the valued of $\nabla_{\lambda_l} \Gamma$, $\nabla_{\mu_l} \Gamma$, $\nabla_{v_l} \Gamma$, and $\nabla_{\pi_l} \Gamma$ are greater than zero, then λ_l, μ_l, v_l, and π_l decrease. Therefore, one can employ the binary search algorithm of error ϵ_2 to solve and find the optimal Lagrange multipliers $(v^*, \pi^*, \lambda^*, \mu^*)$. As a result, the method constructed in steps 1 and 2 alternately work until the duality differences are constant, i.e.,

$$
|R_{sum}(\boldsymbol{\rho}^*) - \Gamma(v^*, \pi^*, \lambda^*, \mu^*)| = Constant
\tag{35}
$$

Secondly, one can find the power allocation under a fixed power splitting factor in the optimization problem (15). The purpose is to investigate the optimized power splitting

value ρ^* and the power allocation $p_{l,m} \ \forall \, l,m$. However, the optimization issue in (15) can be written in the following form:

$$P4: \quad \max_{\{p_{l,m}\}} R(p_{l,m}) \tag{36}$$

$$s.t. \quad \sum_{m=1}^{M}\sum_{l=1}^{S_m} P_l \leq P_T \tag{36a}$$

$$e_{l,m} \geq E_{min}, \ \forall \, l,m, \tag{36b}$$

$$R_{l,m}^{ID} \geq R_{min}, \ \forall \, l,m, \tag{36c}$$

$$p_{l,m} \geq 0 \ \forall \, l,m, \tag{36d}$$

To that end, let us assume that the noise power for all devices is equal, i.e., $\left|\sigma_{l,m}\right|^2 \to 0$. Then, one can rewrite the objective function as follows:

$$R(\boldsymbol{p}) = \sum_{m=1}^{M}\sum_{l=1}^{S_m} R_{l,m} \tag{37}$$

$$
\begin{aligned}
R(\boldsymbol{p}) &= \sum_{m=1}^{M}\sum_{l=1}^{S_m} log_2\left(1 + \frac{\rho_l\left|h_{l,m}\right|^2 p_l}{\rho_l\left|h_l\right|^2 \sum_{i=l+1}^{S_m} p_{i,m}+\sigma^2}\right) + \tau \sum_{m=1}^{M}\sum_{l=1}^{S_m} log_2\left(1 + \frac{\gamma\eta(1-\rho_l)\left|h_{l,m}\right|^2 \sum_{m=1}^{M}\sum_{l=1}^{S_m} p_{l,m}}{\sigma^2}\right) \\
&= \sum_{m=1}^{M}\sum_{l=1}^{S_m} log_2\left(1 + \frac{\rho_l\left|h_{l,m}\right|^2 p_{l,m}}{\rho_l\left|h_{l,m}\right|^2 \sum_{i=l+1}^{S_m} p_i+\sigma^2}\right) + \tau log_2\left(1 + \frac{\gamma\eta(1-\rho_l)\left|h_{l,m}\right|^2 P_T}{\sigma^2}\right)
\end{aligned}
\tag{38}
$$

Also, one can rewrite the desired data rate of device l in the following form:

$$R_l = log_2\left(1 + \frac{\left|h_{l,m}\right|^2 p_{l,m}}{\left|h_{l,m}\right|^2 \sum_{i=l+1}^{N} p_i + \sigma^2}\right) \tag{39}$$

$$R_l = \sum_{l=1}^{S_m} log_2\left(1 + \frac{\left|h_{\psi(l)}\right|^2 p_{\psi(l)}}{\left|h_{\psi(l)}\right|^2 \sum_{i=\psi(l)+1}^{S_m} p_i + \sigma^2}\right) \tag{40}$$

where $\psi(l)$ represents the decoding order of the l-th device.

Assume that $\Theta_l = \sum_{j=l}^{S_m} p_{\psi(j)}$ and $\Theta_{l+1} = \sum_{j=l+1}^{S_m} p_{\psi(j)}$. Then, one can rewrite the R_l given in (40) as follows:

$$R_l = \sum_{l=1}^{S_m} log_2\left(\left|h_{\psi(l)}\right|^2 \Theta_l + \sigma^2\right) - \sum_{l=1}^{S_m} log_2\left(\left|h_{\psi(l)}\right|^2 \Theta_{l+1} + \sigma^2\right) \tag{41}$$

Then, the first derivative of R_l in regards to $p_{\psi(l)}$ can be expressed as
Case I: $l = 1$,

$$\frac{\partial R_l}{\partial p_{\psi(l)}} = \frac{1}{ln2} \cdot \frac{\left|h_{\psi(1)}\right|^2}{\left(\left|h_{\psi(1)}\right|^2 \Theta_1 + \sigma^2\right)}, \tag{42}$$

Case II: $2 \leq l \leq S_m$,

$$\frac{\partial R_l}{\partial p_{\psi(l)}} = \frac{1}{ln2} \cdot \left(\frac{\left|h_{\psi(1)}\right|^2}{\left(\left|h_{\psi(1)}\right|^2 \Theta_1 + \sigma^2\right)} + \sum_{j=2}^{l}\left(\frac{\left|h_{\psi(j)}\right|^2}{\left(\left|h_{\psi(j)}\right|^2 \Theta_j + \sigma^2\right)} - \frac{\left|h_{\psi(j-1)}\right|^2}{\left(\left|h_{\psi(j-1)}\right|^2 \Theta_j + \sigma^2\right)}\right)\right) \forall \, n \tag{43}$$

Note that the first derivative in (42) is a special case of (43). Nevertheless, one can find the second derivative of R_l as follows:

$$\frac{\partial^2 R_l}{\partial p_{\psi(l)}\partial p_{\psi(k)}} = -\frac{1}{ln2}\cdot\frac{\left|h_{\psi(1)}\right|^4}{\left(\left|h_{\psi(1)}\right|^2\Theta_1+\sigma^2\right)^2} - \frac{1}{ln2}\cdot\sum_{j=2}^{w}\left(\frac{\left|h_{\psi(j)}\right|^4}{\left(\left|h_{\psi(j)}\right|^2\Theta_j+\sigma^2\right)^2} - \frac{\left|h_{\psi(j-1)}\right|^4}{\left(\left|h_{\psi(j-1)}\right|^2\Theta_j+\sigma^2\right)^2}\right) \forall l \quad (44)$$

where $w = \min(l,k)$. According to (43) and (44), the Hessian matrix of R_l can be either zero or negative for $p_{l,m} \forall l,m$. However, the cost function in (36) can be considered as a concave function for all $p_{l,m} \forall l,m$.

To that end, one can express the problem in (36), using the Lagrangian, by:

$$\overline{Y}(p,\tau,o,\kappa,\delta) = \sum_{m=1}^{M}\sum_{l=1}^{S_m}\log_2\left(1+\frac{\left|h_{\psi(n)}\right|^2 p_{\psi(n)}}{\left|h_{\psi(n)}\right|^2\Sigma_{j=n+1}^{N}p_{\psi(j)}+\sigma^2}\right) + \sum_{l=1}^{S_m}\tau_l\left(P_T - \sum_{m=1}^{M}\sum_{l=1}^{S_m}p_{\psi(l)}\right)$$
$$+ \sum_{l=1}^{S_m}o_l\left(\sum_{m=1}^{M}\sum_{l=1}^{S_m}\log_2\left(1+\frac{\gamma E_{min}}{\sigma^2}\right) - \sum_{m=1}^{M}\sum_{l=1}^{S_m}\log_2\left(1+\frac{\gamma\eta(1-\rho_l{}^*)\left|h_{\psi(l)}\right|^2\Sigma_{l=1}^{S_m}p_{\psi(l)}}{\sigma^2}\right)\right) \quad (45)$$
$$+ \sum_{l=1}^{S_m}\kappa_l\left(R_{min} - \sum_{m=1}^{M}\sum_{l=1}^{S_m}\log_2\left(1+\frac{\left|h_{\psi(l)}\right|^2 p_{\psi(l)}}{\left|h_{\psi(l)}\right|^2\Sigma_{j=l+1}^{S_m}p_{\psi(j)}+\sigma^2}\right)\right) + \sum_{l=1}^{S_m}\delta_l\sum_{l=1}^{S_m}p_{\psi(l)}$$

where $\tau = [\tau_1, \tau_2, \ldots, \tau_{S_m}]^T$, $o = [o_1, o_2, \ldots, o_{S_m}]^T$, $\kappa = [\kappa_1, \kappa_2, \ldots, \kappa_{S_m}]^T$ and $\delta = [\delta_1, \delta_2, \ldots, \delta_{S_m}]^T$ denote Lagrange multipliers for the corresponding constraints in (36a), (36b), (36c), and (36d), respectively.

Nevertheless, the Lagrange dual objective function can be expressed as

$$\overline{\Gamma}(\tau, o, \kappa, \delta) = \max_{p}\overline{Y}(p, \tau, o, \kappa, \delta) \quad (46)$$

Then,

$$\min_{\alpha,\eta,\kappa} \quad \overline{\Gamma}(\tau, o, \kappa, \delta) \quad (47)$$

$$s.t. \quad \tau \succeq 0, o \succeq 0, \kappa \succeq 0, \delta \succeq 0. \quad (48)$$

And the first derivative of the Lagrangian function, as a function of power allocation $p_{\psi(l)}$, can be expressed by:

$$\nabla_{p_{\psi(l)}}\overline{Y} = \frac{1}{ln2}\cdot\left(\frac{\left|h_{\psi(1)}\right|^2}{\left(\left|h_{\psi(1)}\right|^2\Theta_1+\sigma^2\right)} + \sum_{j=2}^{l}\left(\frac{\left|h_{\psi(j)}\right|^2}{\left(\left|h_{\psi(j)}\right|^2\Theta_j+\sigma^2\right)} - \frac{\left|h_{\psi(j-1)}\right|^2}{\left(\left|h_{\psi(j-1)}\right|^2\Theta_j+\sigma^2\right)}\right)\right) - \tau_l + \frac{1}{ln2}$$
$$\cdot\left(\sum_{l=1}^{S_m}o_l\gamma\eta(1-\rho_l{}^*)\left|h_{\psi(l)}\right|^2\right) + \frac{\kappa_l}{ln2} \quad (49)$$
$$\cdot\left(\frac{\left|h_{\psi(1)}\right|^2}{\left(\left|h_{\psi(1)}\right|^2\Theta_1+\sigma^2\right)} + \sum_{j=2}^{l}\left(\frac{\left|h_{\psi(j)}\right|^2}{\left(\left|h_{\psi(j)}\right|^2\Theta_j+\sigma^2\right)} - \frac{\left|h_{\psi(j-1)}\right|^2}{\left(\left|h_{\psi(j-1)}\right|^2\Theta_j+\sigma^2\right)}\right)\right) + \delta_l$$

Particularly, one can employ the following formula to update the $p_{\psi(l)}$ as follows:

$$p_{\psi(l)}(Itr+1) = p_{\psi(l)}(Itr) + \overline{\varepsilon}(Itr)\nabla_{p_{\psi(l)}(Itr)}\overline{Y} \quad (50)$$

where $\overline{\varepsilon}(Itr)$ represents the step size, according to (29).

To find the optimal power allocation p^*, the updated process in (50) for the power allocation can be continued till $\left|\nabla_{p_{\psi(l)}}Y\right| \leq \epsilon_3 \forall 1 \leq l \leq S_m$. Therefore, the problem in (46) can be reformulated as

$$\overline{\Gamma}(\tau, o, \kappa, \delta) = \overline{Y}(p^*, \tau, o, \kappa, \delta) \quad (51)$$

Then, one can use the Lagrange dual method to identify Lagrange multipliers $(\tau, o, \kappa, \delta)$ in (47) and (48) as

$$\nabla_{\tau_l}\overline{\Gamma} = P_T - \sum_{m=1}^{M}\sum_{l=1}^{S_m} p_{\psi(l)} \tag{52}$$

$$\nabla_{o_l}\overline{\Gamma} = \sum_{m=1}^{M}\sum_{l=1}^{S_m} log_2\left(1 + \frac{\gamma E_{min}}{\sigma^2}\right) - \sum_{m=1}^{M}\sum_{l=1}^{S_m} log_2\left(1 + \frac{\gamma\eta(1-\rho_l^*)\left|h_{\psi(l)}\right|^2 \sum_{l=1}^{S_m} p_{\psi(l)}}{\sigma^2}\right) \tag{53}$$

$$\nabla_{\kappa_l}\overline{\Gamma} = R_{min} - \sum_{m=1}^{M}\sum_{l=1}^{S_m} log_2\left(1 + \frac{\left|h_{\psi(l)}\right|^2 p_{\psi(l)}}{\left|h_{\psi(l)}\right|^2 \sum_{j=l+1}^{S_m} p_{\psi(j)} + \sigma^2}\right) \tag{54}$$

$$\nabla_{\delta_l}\overline{\Gamma} = p_{\psi(l)} \tag{55}$$

To that end, one can employ the binary search method to find the optimal solution of (51) as follows:

$$\left|R(\boldsymbol{p}^*) - \overline{\Gamma}(\boldsymbol{\tau}^*, \boldsymbol{o}^*, \boldsymbol{\kappa}^*, \boldsymbol{\delta}^*)\right| = Constant \tag{56}$$

Algorithm 1 summarizes the comprehensive methods for solving the optimization problem based on dual Lagrangian methodology. Figure 2 also shows the visualization of your assumed factory environment, including the IIOT connectivity, network infrastructure, and edge connectivity.

Algorithm 1 The presented method for joint optimization problem of resource allocation algorithm and power splitting ratio

---

Input :
        Channel vectors : $h_{l,m} \forall l, m$
        Noise variance : σ^2
       Max iteration : Itr_{max}
Output :
      $p^* = p_{l,m}^* \quad \forall l, m$ **for the** optimized power allocation vector
      $\rho^* = \rho_l^* \forall l$ for for optimized power control vector
1 : Randomly initial power allocations **p** with setting the error tollariance ϵ_1, ϵ_2, $\epsilon_3 = 10^{-4}$
2 : Solve the problem P3 in (16) to optimize $\rho_l \forall l$ with constant power allocation

- Randomly initial dual weights (v, π, λ, μ)
- Find the optimal ρ^* according to (27)–(28)
- If $\left|\nabla_{\rho_l(Itr)} Y\right| \le \epsilon_1 \forall l$, break;
- Find $(v^*, \pi^*, \lambda^*, \mu^*)$ according to Equations in (31)–(34)
- If $|R(\rho^*) - \Gamma(v^*, \pi^*, \lambda^*, \mu^*)| = $ **Constant**; Stop.

9 : Solve the problem P4 in (36) to optimize p^* with the optimal ρ^*

- Randomly initial dual weights $(\tau, o, \kappa, \delta)$
- Find the optimal $\acute{p}*$ according to (49)–(50)
- If $\left|\nabla_{\rho_l(Itr)} Y\right| \le \epsilon_3 \forall l$, Break.
- Find $(\tau^*, o^*, \kappa^*, \delta^*)$ according to Equations in (52)–(55).
- If $\left|R(p^*) - \overline{\Gamma}(\tau^*, o^*, \kappa^*, \delta^*)\right| = $ **Constant** Stop.

---

7. Simulation and Validation of the Energy Efficiency in the Factory of the Future Environments

The simulation results presented in this part are used to verify the performance of the proposed method in the SWIPT NOMA-enabled IIoT networks. The results of the simulations are presented below, along with a discussion of findings. Simulation parameters can be found in the following Table 2 [7,24,33,48,56].

Table 2. Simulation Parameters.

Parameter	Description	Value
σ^2	AWGN variance	0.1
r	The radius of the factory	500 m
d_0	The reference distance	150 m
v	The path-loss exponent	3.76
N	Max. number of IIoT Devices	24
M	Number of sub-channels	8
η	The EH efficiency	0.6
γ	The conversion efficiency	10
τ	The preference weight	0.1
S_m	Number of IIoT devices associated to the sub-channel	2
f	Operating frequency	3.5 GHz
P_t	The total transmission power available at the BS	8 W
P_c	The circuit power	0.2 W
R_{min}	The minimum QoS threshold at the BS	1 b/s/Hz
E_{min}	The minimum harvested power	0.1 m W

All of the results are gathered from a variety of randomly selected locations among the devices. Assume that the BS is positioned in the center of a factory with a radius of $r = 500$ m and that all IIoT devices are dispersed, randomly and independently, inside the factory. The system's overall frequency band is set at $BW = 100$ MHz. The transmission channel between a pair of transceivers in the conventional 3GPP propagation environment [71] consists of i.i.d Rayleigh block fading, Log-Normal shadowing with a standard variation of 8 dB, and path loss given by $\left(\frac{d_0}{d}\right)^v$. Specifically, d represents the actual propagation distance from the BS to the IIoT devices, $d_0 = 50$ m as the reference distance, and $v = 3.76$ represents the path-loss exponent. Other than that, the EH efficiency is set to $\eta = 0.6$, the preference weight is set to $\tau = \frac{a}{b} = 0.1$, and the efficiency of conversion has been set at $\gamma = 10$ percent [7,48,72].

The specifications for the model are as follows: There are a maximum of $N = 24$ IIoT devices and $M = 8$ sub-channels. It is set to $P_t = 8$ W and $R_{min} = 1$ b/s/Hz for the minimal QoS threshold at BS. Each sub-channel has $S_m = 2$ IIoT devices and $P_c = 0.2$ W of circuit power. A variance of $\sigma^2 = 0.1$ is used for the additive white noise. In this paper, the sum rate reached while operating inside a specific spectrum is referred to as spectral efficiency in (56). In contrast, energy efficiency is defined as the ratio of the total power consumed to the sum rate achieved. It can be expressed mathematically as:

$$EE = \frac{Achievable\ sum\ rate}{Total\ power\ consumption} \tag{57}$$

$$EE = \frac{R}{P_t = \sum_{m=1}^{M} \sum_{n=1}^{N} p_{n,m} + P_c} \tag{58}$$

Figure 4 illustrates the energy efficiency as the number of IIoT devices increases. The proposed technique outperforms both the KKT-based NOMA scheme and the standard OFDMA scheme. For fewer IIoT devices, the difference in energy efficiency between the proposed technique and the KKT-based method is insignificant. However, when the number of IIoT devices grows, the gap between the proposed technique and the KKT-based NOMA scheme grows dramatically. On the other hand, the OFDMA-based approach

performs extremely badly when a large number of IIoT devices are deployed. The figure clearly shows that the energy efficiency of the OFDMA scheme achieves saturation when the number of IIoT devices exceeds ten. This is because an OFDMA-based system can handle the same number of IIoT devices as the number of sub-channels, which is set at 10. This demonstrates the OFDMA scheme's failure to manage a high number of IIoT devices, but both NOMA methods continue to improve when the number of IIoT devices exceeds 10.
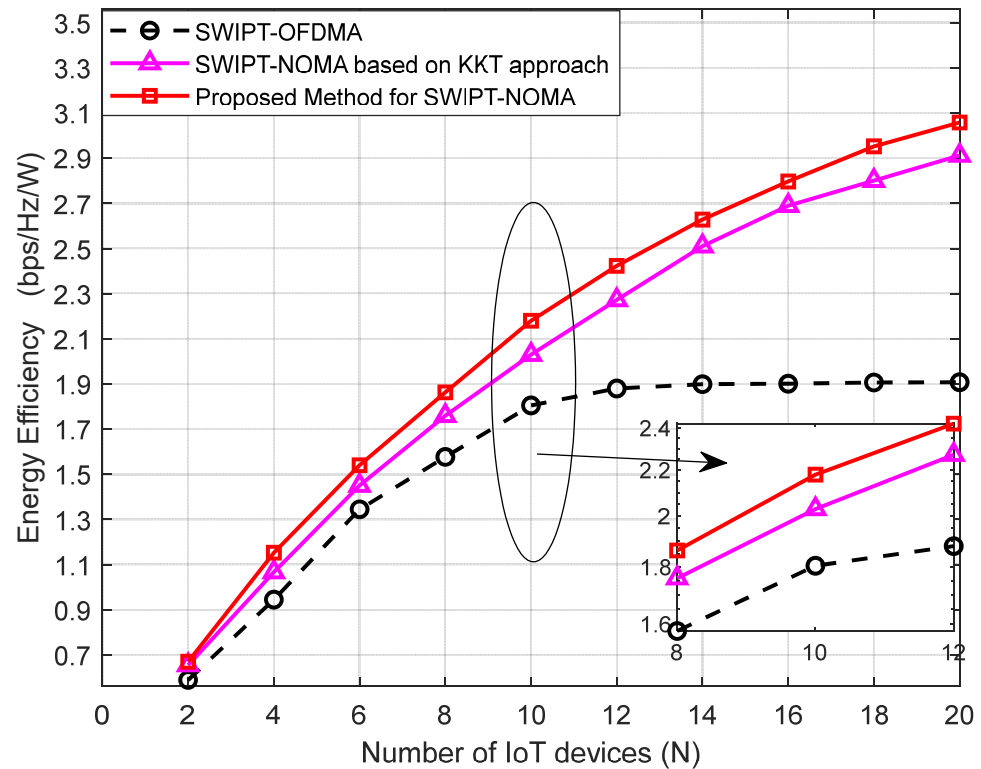

Figure 4. Energy efficiency against the number of IIoT devices.

To study the performance of our proposed scheme further, it is necessary to evaluate the effect of the total transmit power at the BS on the spectral efficiency in (14). The spectral efficiency versus the total power budget at the BS is shown in Figure 5. We can see that the disparity between the curves for the proposed method and the OFDMA-based scheme is rather considerable, indicating that the OFDMA-based scheme performs poorly. Furthermore, we observe that the proposed technique outperforms the benchmark KKT-based NOMA and OFDMA schemes in terms of boosting the BS total power budget.

Figure 6 depicts spectrum efficiency versus total transmit power at the BS with different number of IIoT devices. It compares the proposed NOMA scheme's spectrum efficiency for a different number of IIoT devices. The chart shows the influence of the number of users on optimum spectrum efficiency when the number of users is adjusted to 4, 6, 8, and 10. When the overall transmit power is substantial, as shown in Figure 5, spectrum efficiency improves with the number of users. This is due to the increased diversity gain given when more consumers are serviced concurrently. However, with a low transmit power, spectrum efficiency decreases as the number of users increases. The fundamental cause for this finding is the non-orthogonality of the channel access. Inter-user interference would increase in NOMA systems as the number of terminals increased. This demonstrates that a much greater transmit power is required to meet the minimum rate requirement for each terminal. In other words, limited transmit power cannot fulfill all users' minimal transmission rate needs. As a result, there is a trade-off between spectrum efficiency performance and the number of users, particularly for low-power systems, as in [34].
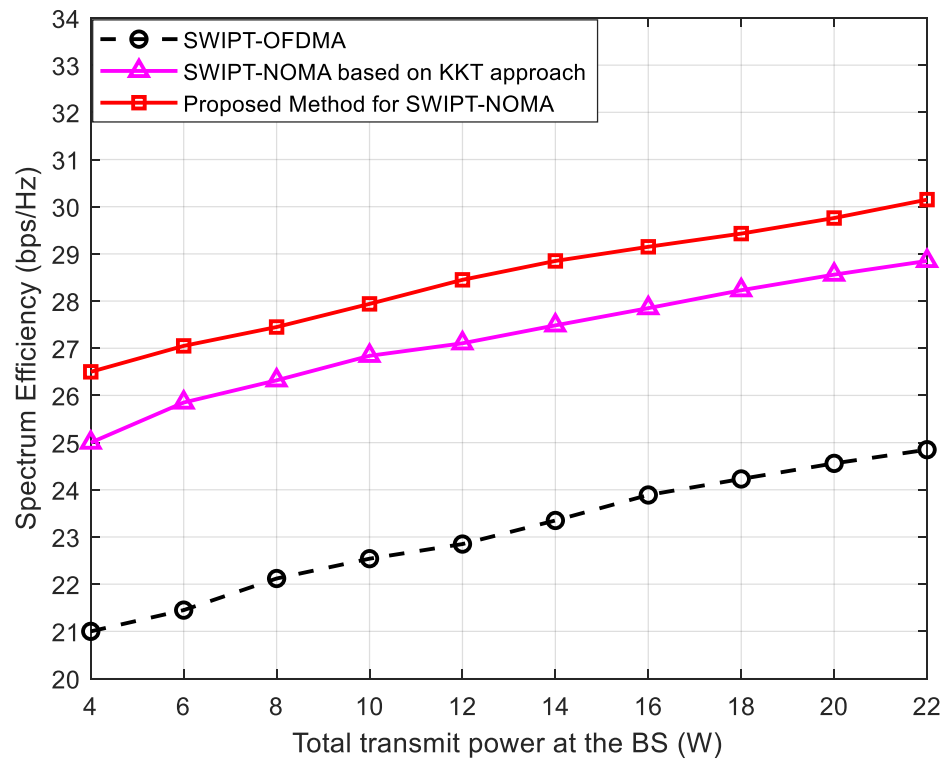
Figure 5. Spectrum efficiency versus total transmit power at the BS.
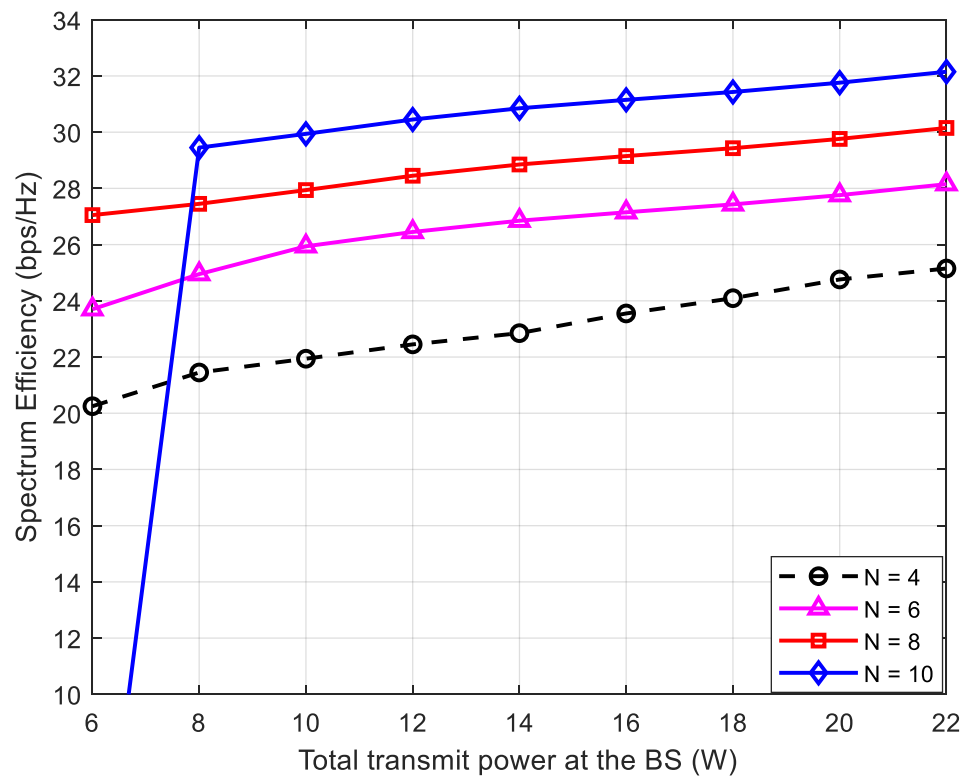

Figure 6. Spectrum efficiency versus total transmit power, at the BS, with different number of IIoT devices.

To demonstrate the performance of the proposed NOMA system with various IIoT devices per sub-channel, Figure 7 analyzes the network's total energy efficiency as the number of sub-channels increases, with each sub-channel capable of accommodating a

different number of IIoT devices at the same time. It can be shown that, as the number of sub-channels increases, so does the total energy efficiency.
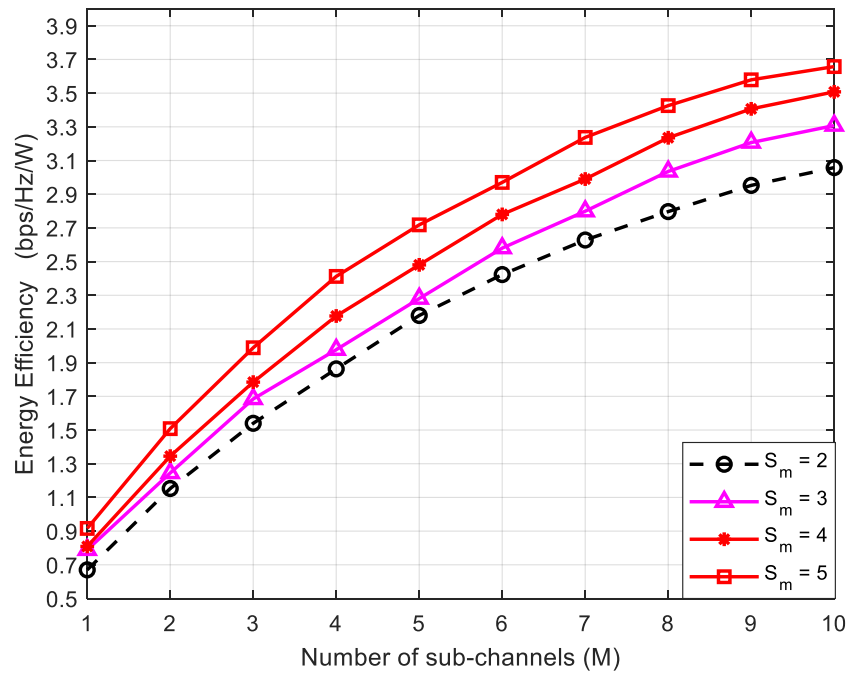

Figure 7. Energy efficiency against the number of sub-channels in the network for different IIoT devices per sub-channel.

It is also worthwhile to illustrate the SE-EE trade-off metric for the presented method in Figure 8. EE and SE have both increased at the same time, showing that no trade-off has occurred over this time period. Once you reach the point of inflection, you will see a decrease in both SE and EE.
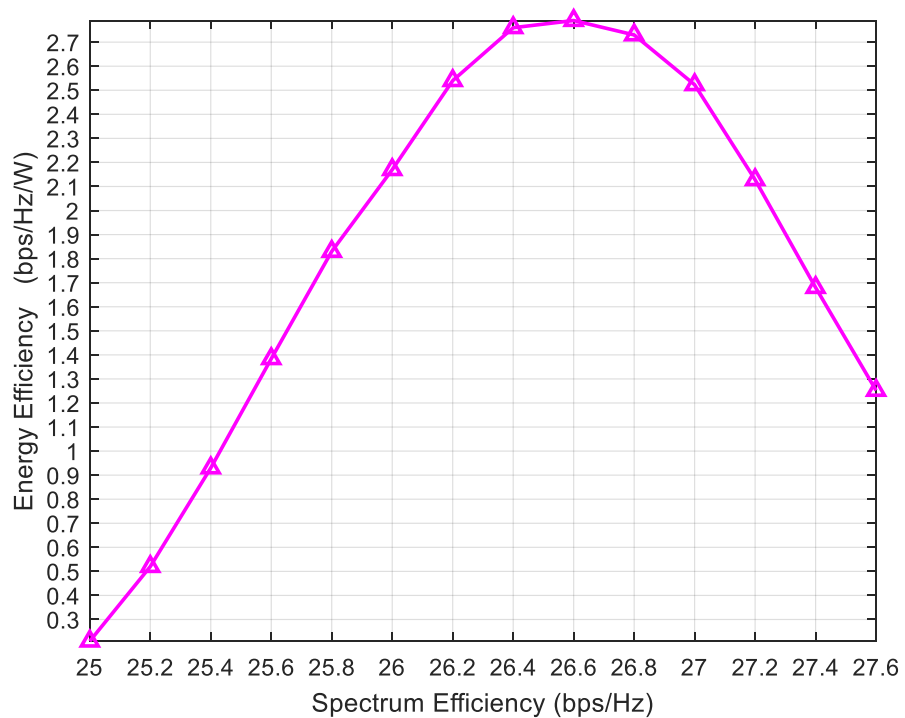

Figure 8. The SE–EE relationship for the proposed system.

8. Conclusions

NOMA is widely regarded as a critical enabler for supporting the massive number of IIoT devices that will be deployed in the factory of the future (FoF). Using the SWIPT-assisted NOMA system with PS receivers as a case study, we looked at the feasible data rate maximization issue under the constraints of the maximum transmit power budget and the minimal EH requirement in this work. For NOMA-enabled IIoT networks, a joint optimization of power allocation and splitting control strategy that is both energy-efficient and cost-effective is presented. The allocation of power and the assignment of the PS ratio were done separately. The Lagrangian duality-based technique was then used to solve the related sub-problems. Finally, we compare the performance of our proposed scheme to that of traditional KKT-based NOMA and SQP-based OFDMA-based schemes. In comparison to the benchmark systems, the performance assessment shows that our proposed scheme is more effective.

Author Contributions: Conceptualization, A.A., R.N., Z.A. and N.F.A.; methodology, A.A., R.N. and N.F.A.; software, A.A. and Z.A.; validation, A.A., R.N., Z.A. and N.F.A.; formal analysis, A.A., R.N., Z.A. and N.F.A.; investigation, A.A., R.N., Z.A. and N.F.A.; data curation, A.A., R.N., Z.A. and N.F.A.; writing—original draft preparation, A.A. and Z.A.; writing—review and editing, A.A., R.N., Z.A. and N.F.A.; visualization, A.A., R.N., Z.A. and N.F.A.; supervision, R.N. and N.F.A.; project administration, R.N. and N.F.A.; funding acquisition, R.N. and N.F.A. All authors have read and agreed to the published version of the manuscript.

Institutional Review Board Statement: Not applicable.

Informed Consent Statement: Not applicable.

Data Availability Statement: The data presented in this study are available on request from the corresponding author.

Conflicts of Interest: The authors declare no conflict of interest.

References

1. Shirvanimoghaddam, M.; Dohler, M.; Johnson, S.J. Massive non-orthogonal multiple access for cellular IoT: Potentials and limitations. *IEEE Commun. Mag.* **2017**, *55*, 55–61. [CrossRef]
2. Kumar, K.S.; Mani, A.S.R.; Sundaresan, S.; Kumar, T.A. *Cloud and IoT-Based Vehicular Ad Hoc Networks*; Wiley: Hoboken, NJ, USA, 2021; p. 105.
3. George, G.; Thampi, S.M. A Graph-Based Security Framework for Securing Industrial IoT Networks from Vulnerability Exploitations. *IEEE Access* **2018**, *6*, 43586–43601. [CrossRef]
4. Zhu, Z.; Li, X.; Chu, Z. *Intelligent Sensing and Communications for Internet of Everything*; Elsevier: Amsterdam, The Netherlands, 2022; p. 15.
5. Wu, Q.; Chen, W.; Ng, D.W.K.; Schober, R. Spectral and Energy-Efficient Wireless Powered IoT Networks: NOMA or TDMA? *IEEE Trans. Veh. Technol.* **2018**, *67*, 6663–6667. [CrossRef]
6. Jabeen, T.; Ali, Z.; Khan, W.U.; Jameel, F.; Khan, I.; Sidhu, G.A.S.; Choi, B.J. Joint Power Allocation and Link Selection for Multi-Carrier Buffer Aided Relay Network. *Electronics* **2019**, *8*, 686. [CrossRef]
7. Khan, W.U.; Jameel, F.; Jamshed, M.A.; Pervaiz, H.; Khan, S.; Liu, J. Efficient power allocation for NOMA-enabled IoT networks in 6G era. *Phys. Commun.* **2020**, *39*, 101043. [CrossRef]
8. Tran, T.-N.; Vo, T.P.; Fazio, P.; Voznak, M. SWIPT Model Adopting a PS Framework to Aid IoT Networks Inspired by the Emerging Cooperative NOMA Technique. *IEEE Access* **2021**, *9*, 61489–61512. [CrossRef]
9. Ribeiro, F.C.; Guerreiro, J.; Dinis, R.; Cercas, F.; Jayakody, D.N.K. Multi-user detection for the downlink of NOMA systems with multi-antenna schemes and power-efficient amplifiers. *Phys. Commun.* **2019**, *33*, 199–205. [CrossRef]
10. Ding, Z.; Lei, X.; Karagiannidis, G.K.; Schober, R.; Yuan, J.; Bhargava, V. A survey on non-orthogonal multiple access for 5G networks: Research challenges and future trends. *IEEE J. Sel. Areas Commun.* **2017**, *35*, 2181–2195. [CrossRef]
11. Ding, Z.; Fan, P.; Poor, H.V. Impact of user pairing on 5G nonorthogonal multiple-access downlink transmissions. *IEEE Trans. Veh. Technol.* **2016**, *65*, 6010–6023. [CrossRef]
12. Chen, Z.; Ding, Z.; Dai, X.; Zhang, R. An optimization perspective of the superiority of NOMA compared to conventional OMA. *IEEE Trans. Signal Process.* **2017**, *65*, 5191–5202. [CrossRef]

13. Chen, R.; Shu, F.; Lei, K.; Wang, J.; Zhang, L. User Clustering and Power Allocation for Energy Efficiency Maximization in Downlink Non-Orthogonal Multiple Access Systems. *Appl. Sci.* **2021**, *11*, 716. [CrossRef]

14. Xu, D.; Li, Q. Resource allocation in OFDM-based wireless powered communication networks with SWIPT. *AEU-Int. J. Electron. Commun.* **2019**, *101*, 69. [CrossRef]

15. Ding, J.; Jiang, L.; He, C.; Shen, Y. Time Splitting Concurrent Transmission Framework and Resource Allocation in Wireless Powered Communication Networks. *IEEE Trans. Green Commun. Netw.* **2018**, *2*, 666–678. [CrossRef]

16. Ding, Z.; Fan, P.; Poor, H.V. Impact of Non-Orthogonal Multiple Access on the Offloading of Mobile Edge Computing. *Commun. IEEE Trans. Green Commun. Netw.* **2019**, *67*, 375–390. [CrossRef]

17. Zhou, X.; Li, J.; Shu, F.; Wu, Q.; Wu, Y.; Chen, W.; Hanzo, L. Secure SWIPT for Directional Modulation-Aided AF Relaying Networks. *IEEE J. Sel. Areas Commun.* **2019**, *37*, 253–268. [CrossRef]

18. Fadhil, M.; Abdullah, N.F.; Ismail, M.; Nordin, R.; Saif, A.; Al-Obaidi, M. Power Allocation in Cooperative NOMA MU-MIMO Beamforming Based on Maximal SLR Precoding for 5G. *J. Commun.* **2019**, *14*, 676–683. [CrossRef]

19. Lim, H.; Hwang, T. User-Centric Energy Efficiency Optimization for MISO Wireless Powered Communications. *IEEE Trans. Wirel. Commun.* **2019**, *18*, 864–878. [CrossRef]

20. Qian, L.P.; Feng, A.; Huang, Y.; Wu, Y.; Ji, B.; Shi, Z. Optimal SIC Ordering and Computation Resource Allocation in MEC-Aware NOMA NB-IoT Networks. *Internet Things J. IEEE* **2019**, *6*, 2806–2816. [CrossRef]

21. Liu, M.; Song, T.; Gui, G. Deep Cognitive Perspective: Resource Allocation for NOMA-Based Heterogeneous IoT with Imperfect SIC. *Internet Things J. IEEE* **2019**, *6*, 2885–2894. [CrossRef]

22. Zhao, N.; Pang, X.; Li, Z.; Chen, Y.; Li, F.; Ding, Z.; Alouini, M. Joint Trajectory and Precoding Optimization for UAV-Assisted NOMA Networks. *IEEE Trans. Commun.* **2019**, *67*, 3723–3735. [CrossRef]

23. Yu, Z.; Chi, K.; Zheng, K.; Li, Y.; Cheng, Z. Transmit power allocation of energy transmitters for throughput maximisation in wireless powered communication networks. *Commun. IET* **2019**, *13*, 1200–1206. [CrossRef]

24. Zhou, X.; Zhang, R.; Ho, C.K. Wireless information and power transfer in multiuser OFDM systems. *IEEE Trans. Wirel. Commun.* **2014**, *13*, 2282–2294. [CrossRef]

25. Andrawes, A.; Nordin, R.; Abdullah, N.F. Energy-Efficient Downlink for Non-Orthogonal Multiple Access with SWIPT under Constrained Throughput. *Energies* **2020**, *13*, 107. [CrossRef]

26. Hu, Y.; Zhu, Y.; Gursoy, M.C.; Schmeink, A. SWIPT-enabled relaying in IoT networks operating with finite blocklength codes. *IEEE J. Sel. Areas Commun.* **2019**, *37*, 74–88. [CrossRef]

27. Lu, W.; Gong, Y.; Wu, J.; Peng, H.; Hua, J. Simultaneous wireless information and power transfer based on joint subcarrier and power allocation in OFDM systems. *IEEE Access* **2017**, *5*, 2763–2770. [CrossRef]

28. Albataineh, Z.; Salem, F. Blind multiuser detection based on the fast relative newton algorithm. In *2014 Wireless Telecommunications Symposium*; IEEE: Piscataway, NJ, USA, 2014; pp. 1–5.

29. Xu, Y.; Shen, C.; Ding, Z.; Sun, X.; Yan, S.; Zhu, G.; Zhong, Z. Joint beamforming and power-splitting control in downlink cooperative SWIPT NOMA systems. *IEEE Trans. Signal Process.* **2017**, *65*, 4874–4886. [CrossRef]

30. Sun, H.; Zhou, F.; Hu, R.Q.; Hanzo, L. Robust beamforming design in a NOMA cognitive radio network relying on SWIPT. *IEEE J. Sel. Areas Commun.* **2019**, *37*, 142–155. [CrossRef]

31. Jang, S.; Lee, H.; Kang, S.; Oh, T.; Lee, I. Energy efficient SWIPT systems in multi-cell MISO networks. *IEEE Trans. Wirel. Commun.* **2018**, *17*, 8180–8194. [CrossRef]

32. Xiang, Z.; Li, Q. Energy efficiency for SWIPT in MIMO two-way amplify-and-forward relay networks. *IEEE Trans. Veh. Technol.* **2018**, *67*, 4910–4924.

33. Diamantoulakis, P.D.; Pappi, K.N.; Ding, Z.; Karagiannidis, G.K. Wireless-powered communications with non-orthogonal multiple access. *IEEE Trans. Wirel. Commun.* **2016**, *15*, 8422–8436. [CrossRef]

34. Tang, J.; Yu, Y.; Liu, M.; So, D.K.; Zhang, X.; Li, Z.; Wong, K.K. Joint Power Allocation and Splitting Control for SWIPT-Enabled NOMA Systems. *IEEE Trans. Wirel. Commun.* **2020**, *19*, 120–133. [CrossRef]

35. Liu, Y.; Chen, X.; Cai, L.X.; Chen, Q.; Gong, R.; Tang, D. On the Fairness Performance of NOMA-Based Wireless Powered Communication Networks. In Proceedings of the ICC 2019—2019 IEEE International Conference on Communications (ICC), Shanghai, China, 20–24 May 2019; pp. 1–6.

36. Yu, Z.; Chi, K.; Hu, P.; Zhu, Y.; Liu, X. Energy Provision Minimization in Wireless Powered Communication Networks with Node Throughput Requirement. *IEEE Trans. Veh. Technol.* **2019**, *68*, 7057–7070. [CrossRef]

37. Shahini, A.; Ansari, N. NOMA Aided Narrowband IoT for Machine Type Communications with User Clustering. *Internet Things J. IEEE* **2019**, *6*, 7183–7191. [CrossRef]

38. Bhat, a.V.; Motani, M.; Lim, T.J. Hybrid NOMA for an Energy Harvesting MAC With Non-Ideal Batteries and Circuit Power. *IEEE Trans. Wirel. Commun.* **2019**, *18*, 3961–3973. [CrossRef]

39. Karthika, E.; Mohanapriya, S. Dynamic Clustering-Genetic Secure Energy Awareness Routing to Improve the Performance of Energy Efficient in IoT Cloud. *IOP Conf. Ser. Mater. Sci. Eng.* **2020**, *995*, 012035. [CrossRef]

40. Tan, T.; Yan, Z.; Zou, H.; Ma, K.; Liu, F.; Zhao, L.; Peng, Z.; Zhang, W. Renewable energy harvesting and absorbing via multi-scale metamaterial systems for Internet of things. *Appl. Energy* **2019**, *254*, 113717. [CrossRef]

41. Andrawes, A.; Nordin, R.; Ismail, M. Wireless Energy Harvesting with Amplify-and-Forward Relaying and Link Adaptation under Imperfect Feedback Channel. *J. Telecommun. Electron. Comput. Eng.* **2018**, *10*, 83–90.

42. Qureshi, B.; Aziz, S.A.; Wang, X.; Hawbani, A.; Alsamhi, S.H.; Qureshi, T.; Naji, A. A state-of-the-art survey on wireless rechargeable sensor networks: Perspectives and challenges. *Wirel. Netw.* **2022**. [CrossRef]

43. Li, X.; Luo, C.; Ji, H.; Zhuang, Y.; Zhang, H.; Leung, V.C.M. Energy consumption optimization for self-powered IoT networks with non-orthogonal multiple access. *Int. J. Commun. Syst.* **2020**, *33*, e4174. [CrossRef]

44. Balcı, A.; Sokullu, R. Massive connectivity with machine learning for the Internet of Things. *Comput. Netw.* **2021**, *184*, 107646. [CrossRef]

45. Farooq, M.U.; Wang, X.; Hawbani, A.; Khan, A.; Ahmed, A.; Alsamhi, S.; Qureshi, B. POWER: Probabilistic weight-based energy-efficient cluster routing for large-scale wireless sensor networks. *J. Supercomput.* **2020**, *78*, 12765–12791. [CrossRef]

46. Andrawes, A.; Nordin, R.; Ismail, M. Energy Harvesting with Link Adaptation under Different Wireless Relaying Schemes. *J. Commun.* **2018**, *13*, 482–489. [CrossRef]

47. Azarhava, H.; Abdollahi, M.P.; Niya, J.M. Age of information in wireless powered IoT networks: NOMA vs. TDMA. *Ad Hoc Netw.* **2021**, *104*, 102179. [CrossRef]

48. Rauniyar, A.; Engelstad, P.; Østerbø, O.N. Ergodic sum capacity analysis of NOMA-SWIPT enabled IoT relay systems. *Internet Technol. Lett.* **2021**, *4*, e218. [CrossRef]

49. Tang, J.; Luo, J.; Ou, J.; Zhang, X.; Zhao, N.; So, D.K.C.; Wong, K.K. Decoupling or Learning: Joint Power Splitting and Allocation in MC-NOMA with SWIPT. *IEEE Trans. Commun.* **2020**, *68*, 5834–5848. [CrossRef]

50. Jawarneh, A.; Kadoch, M.; Albataineh, Z. Decoupling Energy Efficient Approach for Hybrid Precoding-Based mmWave Massive MIMO-NOMA with SWIPT. *IEEE Access* **2022**, *10*, 28868–28884. [CrossRef]

51. Salh, A.; Audah, L.; Abdullah, Q.; Aydoğdu, Ö.; Alhartomi, M.A.; Alsamhi, S.H.; Almalki, F.A.; Shah, N.S.M. Low Computational Complexity for Optimizing Energy Efficiency in mm-wave Hybrid Precoding System for 5G. *IEEE Access* **2022**, *10*, 4714–4727. [CrossRef]

52. Zavyalova, D.; Drozdova, V. 5G scheduling using reinforcement learning. In Proceedings of the 2020 International Multi-Conference on Industrial Engineering and Modern Technologies (FarEastCon), Vladivostok, Russia, 6–9 October 2020.

53. Li, Z.; Uusitalo, M.A.; Shariatmadari, H.; Singh, B. 5G URLLC: Design challenges and system concepts. In Proceedings of the 2018 15th International Symposium on Wireless Communication Systems (ISWCS), Lisbon, Portugal, 28–31 August 2018.

54. Andrawes, A.; Nordin, R.; Albataineh, Z.; Alsharif, M.H. Sustainable Delay Minimization Strategy for Mobile Edge Computing Offloading under Different Network Scenarios. *Sustainability* **2021**, *13*, 12112. [CrossRef]

55. Santos, P.M.; Rodrigues, J.G.; Cruz, S.B.; Lourenço, T.; d'Orey, P.M.; Luis, Y.; Rocha, C.; Sousa, S.; Crisóstomo, S.; Queirós, C.; et al. PortoLivingLab: An IoT-based sensing platform for smart cities. *IEEE Internet Things J.* **2018**, *5*, 523–532. [CrossRef]

56. Nguyen, T.-D.; Huh, E.-N.; Jo, M. Decentralized and revised content-centric networking-based service deployment and discovery platform in mobile edge computing for IoT devices. *IEEE Internet Things J.* **2018**, *6*, 4162–4175. [CrossRef]

57. Di, B.; Song, L.; Li, Y. Sub-Channel Assignment, Power Allocation, and User Scheduling for Non-Orthogonal Multiple Access Networks. *IEEE Trans. Wirel. Commun.* **2016**, *15*, 7686–7698. [CrossRef]

58. Singh, K.; Wang, K.; Biswas, S.; Ding, Z.; Khan, F.A.; Ratnarajah, T. Resource optimization in full duplex non-orthogonal multiple access systems. *IEEE Trans. Wirel. Commun.* **2019**, *18*, 4312–4325. [CrossRef]

59. Yu, G.; Jiang, Y.; Xu, L.; Li, G.Y. Multi-objective energy-efficient resource allocation for multi-RAT heterogeneous networks. *IEEE J. Sel. Areas Commun.* **2015**, *33*, 2118–2127. [CrossRef]

60. Hsu, C.-W.; Hsu, Y.-L.; Wei, H.-Y. Energy-efficient edge offloading in heterogeneous industrial IoT networks for factory of future. *IEEE Access* **2020**, *8*, 183035–183050. [CrossRef]

61. Wang, H.; Yemeni, Z.; Ismael, W.M.; Hawbani, A.; Alsamhi, S.H. A reliable and energy efficient dual prediction data reduction approach for WSNs based on Kalman filter. *IET Commun.* **2021**, *15*, 2285–2299. [CrossRef]

62. Hsu, C.-W.; Hsu, Y.-L.; Wei, H.-Y. Energy-efficient and reliable MEC offloading for heterogeneous industrial IoT networks. In Proceedings of the 2019 European Conference on Networks and Communications (EuCNC), Valencia, Spain, 18–21 June 2019.

63. Yeom, K.-R.; Choi, H.-S. Prediction of Manufacturing Plant's Electric Power Using Machine Learning. In Proceedings of the 2018 Tenth International Conference on Ubiquitous and Future Networks (ICUFN), Prague, Czech Republic, 3–6 July 2018.

64. Albataineh, Z. Blind Decoding of Massive MIMO Uplink Systems Based on the Higher Order Cumulants. *Wirel. Pers. Commun.* **2018**, *103*, 1835–1847. [CrossRef]

65. Blanchet, T.; Chancel, L.; Gethin, A. How unequal is Europe? Evidence from distributional national accounts, 1980–2017. In *WID. World Working Paper*; The World Inequality Lab.: Paris, France, 2019; Volume 6.

66. Saif, A.; Dimyati, K.; Noordin, K.A.; Shah, N.S.M.; Alsamhi, S.H.; Abdullah, Q. Energy-Efficient Tethered UAV Deployment in B5G for Smart Environments and Disaster Recovery. In Proceedings of the 2021 1st International Conference on Emerging Smart Technologies and Applications (eSmarTA), Sana'a, Yemen, 10–12 August 2021; pp. 1–5.

67. Chaudhri, S.N.; Rajput, N.S.; Alsamhi, S.H.; Shvetsov, A.V.; Almalki, F.A. Zero-Padding and Spatial Augmentation-Based Gas Sensor Node Optimization Approach in Resource-Constrained 6G-IoT Paradigm. *Sensors* **2022**, *22*, 3039. [CrossRef]

68. Karnouskos, S.; Colombo, A.W.; Lastra, J.L.M.; Popescu, C. Towards the energy efficient future factory. In Proceedings of the 2009 7th IEEE International Conference on Industrial Informatics, Cardiff, UK, 23–26 June 2009.

69. Weidlich, A.; Vogt, H.; Krauss, W.; Spiess, P.; Jawurek, M.; Johns, M.; Karnouskos, S. Decentralized intelligence in energy efficient power systems. In *Handbook of Networks in Power Systems I*; Springer: Berlin/Heidelberg, Germany, 2012; pp. 467–486.

70. Albataineh, Z. Low-Complexity Near-Optimal Iterative Signal Detection Based on MSD-CG Method for Uplink Massive MIMO Systems. *Wirel. Pers. Commun.* **2012**, *116*, 2549–2563. [CrossRef]
71. Boyd, S.; Vandenberghe, L. *Convex Optimization*; Cambridge University Press: Cambridge, UK, 2004.
72. GreenTouch, Mobile Communications WG Architecture doc2: Reference Scenarios. May 2013. Available online: https://citeseerx.ist.psu.edu/viewdoc/download;jsessionid=A7176B89E1B08CF2F97232D94BFE6CBD?doi=10.1.1.678.501&rep=rep1&type=pdf (accessed on 29 June 2022).